



Cite this: *Chem. Sci.*, 2023, **14**, 14020

All publication charges for this article have been paid for by the Royal Society of Chemistry

Received 5th October 2023

Accepted 8th November 2023

DOI: 10.1039/d3sc05272a

rsc.li/chemical-science

Dipyrrolonaphthyridinedione – (still) a mysterious cross-conjugated chromophore

Bartłomiej Sadowski ^{*a} and Daniel T. Gryko ^{*b}

Dipyrrolonaphthyridinediones (DPNDs) entered the chemical world in 2016. This cross-conjugated donor-acceptor skeleton can be prepared in two steps from commercially available reagents in overall yield $\approx 15\text{--}20\%$ (5 mmol scale). DPNDs can be easily and regioselectively halogenated which opens an avenue to numerous derivatives as well as to π -expansion. Although certain synthetic limitations exist, the current derivatization possibilities provided impetus for numerous explorations that use DPNDs. Structural modifications enable bathochromic shift of the emission to deep-red region and reaching the optical brightness $30\,000\text{ M}^{-1}\text{ cm}^{-1}$. Intense absorption and strong emission of greenish-yellow light attracted the interest which eventually led to the discovery of their strong two-photon absorption, singlet fission in the crystalline phase and triplet sensitization. Dipyrrolonaphthyridinedione-based twistacenes broadened our knowledge on the influence of twisting angle on the fate of the molecule in the excited state. Collectively, these findings highlight the compatibility of DPNDs with various applications within organic optoelectronics.

1. Introduction

A pyrrole ring is probably the most known small aromatic heterocycle. Many of its derivatives are found in a variety of natural products¹ as well as drugs.² In addition, this small heterocyclic motif is a key part of many functional dyes such as porphyrinoids,³ corroles,⁴ indolizines,⁵ 4,4-difluoro-4-bora-3a,4a-diaza-s-indacene (BODIPY)⁶ or bis(difluoroboron)-1,2-bis((1*H*-pyrrol-2-yl)methylene)hydrazine (BOPHY).⁷

Due to its intrinsic electron-rich character, a pyrrole ring seems to be an ideal candidate for an electron-donating moiety in cross-conjugated chromophores. However, there is still

a huge gap in the understanding of its nature when coupled with electron-accepting units. Some of the recent reports discussed an issue of aromaticity of cross-conjugated chromophores containing a pyrrole ring in a ground and excited singlet/triplet states.⁸

Donor-acceptor cross-conjugated dyes are well established in the literature.⁹ Compounds of this type, *i.e.* diketopyrrolo-pyrroles,¹⁰ isoindigos,¹¹ cibalakrot^{8a,b,12} were tested as main components in organic electronics¹³ or biology.¹⁴ Donor-acceptor systems of cross-conjugated nature also played formidable role in human history. Indigo and Tyrian Purple (6,6'-dibromoindigo) were used as garment dyes for millennia.¹⁵ Moving to modern times, a diketopyrrolopyrrole molecule discovered by Farnum¹⁶ in 1974 and commercialized by Ciba Geigy,¹⁷ is a key structural motif of Pigment Red 254 – better known as ‘Ferrari Red’ as it was used to paint iconic Ferrari cars. Since then, there was no discovery of new type of donor-

^aCentre of New Technologies, University of Warsaw, S. Banacha 2c, 02-097 Warsaw, Poland. E-mail: b.sadowski@cent.uw.edu.pl

^bInstitute of Organic Chemistry, Polish Academy of Sciences, Kasprzaka 44/52, 01-224 Warsaw, Poland. E-mail: dtgryko@icho.edu.pl

Bartłomiej Sadowski was educated in chemistry at the Warsaw University of Technology, Poland. He then obtained his PhD from the Institute of Organic Chemistry of the Polish Academy of Sciences in 2019 under the supervision of Prof. Daniel T. Gryko. After completing his post-doctoral work at Georg-August-Universität Göttingen in the group of Prof. Lutz Ackermann, he began his independent career at Centre of New Technologies, University of Warsaw. His research interests focus on the electrochemically-enabled synthesis of high energy intermediates as well as chemistry of functional aromatic molecules, notably dipyrrolonaphthyridinediones.

Daniel T. Gryko obtained his PhD from the Institute of Organic Chemistry of the Polish Academy of Sciences in 1997, under the supervision of Prof. J. Jurczak. After a post-doctoral stay with Prof. J. Lindsey at North Carolina State University (1998–2000), he started his independent career in Poland. He became Full Professor in 2008. The same year he received the Society of Porphyrins and Phthalocyanines Young Investigator Award and in 2017 Foundation for Polish Science Award. His current research interests are focused on the synthesis of functional dyes as well as on two-photon absorption, solvatofluorochromism, excited-state intramolecular proton transfer and fluorescence probes.



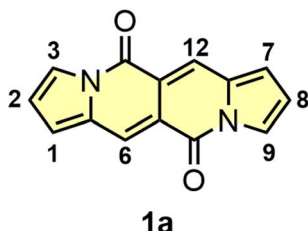


Fig. 1 The structure and numbering of key positions of the simplest dye belonging to the DPND family.

acceptor cross-conjugated dye. The unveiling of dipyrrolonaphthiridinediones (DPNDs) in our research group in 2016 has changed this situation (Fig. 1).¹⁸ The combination of very interesting and unique photophysical properties, straightforward synthesis as well as huge potential for functionalization are responsible for their career in the literature.

In this Perspective article, we will describe the beginnings as well as the history of DPNDs. First of all, we will briefly discuss the synthetic pathways leading to the core followed by describing already known synthetic modifications thereof. Finally, optoelectronic properties will be studied with special emphasis given to structure–property relationship followed by specific applications that has been tested until now. We believe that such structure of the Perspective will open up new avenues for this interesting and still undiscovered chromophore.

2. Synthesis of dipyrrolonaphthiridinediones

The DPND core (Fig. 1) features a 5,6,6,5-type architecture and is comprised of four linearly-fused cycles: two pyrrole rings at the periphery and two six-membered rings in the central part of a chromophore, each containing a C=O group.¹⁸ From the structural point of view, the DPND core closely resembles the BOPHY fluorophore,⁷ however the latter bears BF_2 moieties along with the bis-nitrogen bridge which results in different optoelectronic behavior.

Accordingly to X-ray analysis of **1f** (see Table 1 and Fig. 2),¹⁸ the core is rigidly planar and deviations from the plane are no greater than 0.018 Å. Undoubtedly, the steric clash between C=O groups and alkyl chains at positions 6 and 12 has detrimental influence on the chromophore structure as bond angles between C=O groups and carbon atoms adjacent to the alkyl groups deviate significantly from their ideal trigonal values of 120°. The values are closer to 120° in the case of **1a** that lacks alkyl chains at positions 6 and 12, as revealed by Wang and others¹⁹ (*vide infra*).

Initial attempts to assemble the DPND core were based on the use of 2-formylpyrrole (2) and succinyl chloride (3) as simple and commercially available building blocks, however **1a** could be isolated in only 3.4–6.4% yield along with unreacted 2 and a large amount of black precipitate in both cases (Scheme 1).¹⁸ The presence of the black precipitate was associated with base-

Table 1 Synthesis of various 6,12-disubstituted DPND derivatives^a

Carboxylic acid	Reaction time [h]	DPND	R	Yield [%]	Ref.
$\text{CH}_3\text{CO}_2\text{H}$	5	1b	CH_3	17	18
$\text{C}_7\text{H}_{15}\text{CO}_2\text{H}$	3	1c	C_7H_{15}	29	18
				23 ^b	18
$\text{Et}(\text{Me})\text{CHCO}_2\text{H}$	6	1d	<i>sec</i> -Butyl	21	18
$4-(\text{MeO})_2\text{C}_6\text{H}_4\text{CH}_2\text{CO}_2\text{H}$	6	1e	4-Methoxy-benzyl	10	18
$(\text{C}_2\text{H}_5\text{CO})_2\text{O}^c$	2	1f	C_2H_5	23	18
$\text{C}_3\text{H}_7\text{COOH}$	4	1g	C_3H_7	21	21
$\text{C}_6\text{H}_{13}\text{COOH}$	2	1h	C_6H_{13}	32	19
$2-\text{NO}_2\text{C}_6\text{H}_4\text{COOH}$	3	1i	$2-\text{NO}_2\text{C}_6\text{H}_4$	0	— ^d
$2-\text{ThienylCH}_2\text{COOH}$	3	1j	$2-\text{ThienylCH}_2$	0	— ^d
$3,4-(\text{MeO})_2\text{C}_6\text{H}_4\text{CH}_2\text{CO}_2\text{H}$	3	1k	3,4-Dimethoxy-benzyl	0	— ^d
(<i>E</i>)-Cinnamic acid	3	1l	$-\text{C}=\text{C}-\text{Ph}$	0	— ^d
PhCOOH	3	1m	Ph	0	— ^d
$2-\text{ThienylCH}_2\text{COOH}$	3	1n	$2-\text{ThienylCH}_2$	0	— ^d
$\text{HOOC}(\text{CH}_2)_7\text{COOH}$	3	1o	$-(\text{CH}_2)_7-$	3	20
$\text{HOOC}(\text{CH}_2)_8\text{COOH}$	3	1p	$-(\text{CH}_2)_8-$	15	20
$\text{HOOC}(\text{CH}_2)_9\text{COOH}$	3	1r	$-(\text{CH}_2)_9-$	3	20

^a Reagents proportions: **4** (0.5 mmol), carboxylic acid (3 mmol), TFAA (6 mmol), TFA (3 mmol). ^b 5 mmol scale. ^c Propionic anhydride was used instead of carboxylic acid. ^d Unpublished results.



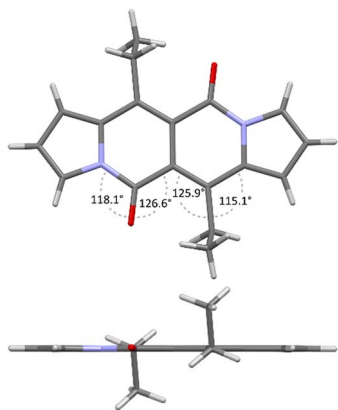
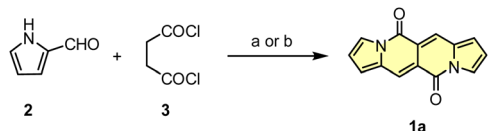


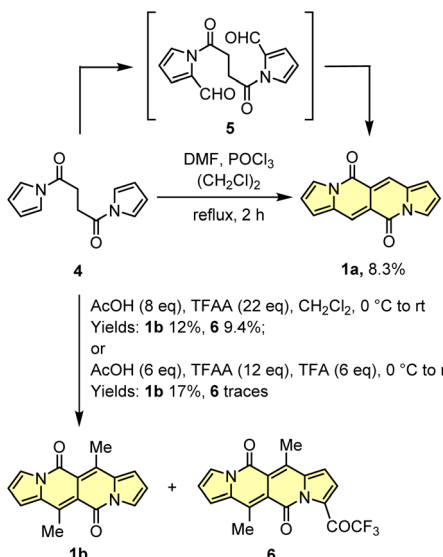
Fig. 2 X-ray structure of compound **1f**. Views perpendicular (top) and along (bottom) with respect to the chromophore plane. Adapted with permission from ref. 18. Copyright 2016 Royal Society of Chemistry.



Scheme 1 Initial attempts of the synthesis of DPND derivatives. Reaction conditions: (a) DMAP (20 mol%), Et_3N , CH_2Cl_2 , rt, 2 h. Yield: 3.4%; (b) K_2CO_3 , DMF, 0 °C, 2 h. Yield: 6.4%.

mediated polymerization of **3** as its formation was also noted in the absence of the aldehyde.

Another tested strategy towards **1a** involved dipyrrroyl derivative **4** as a source of pyrrole rings. Compound **4** can be easily synthesized from either 2,5-dimethoxytetrahydrofuran and succinamide^{18,20} or pyrrole and **3**.²¹ Indeed, subjecting **4** to the typical Vilsmeier-Haack reaction conditions (DMF/ POCl_3) resulted in the formation of **1a**, but still with low efficiency



Scheme 2 Synthesis of DPNDs via acylation of a pyrrole ring.

(Scheme 2). During the optimization process, intermediate of type **5** was not detected at all.

Due to low efficiencies and relatively poor solubility of **1a** in common organic solvents, we intended to introduce additional substituents that improve solubility of resulted chromophores. This idea was realized *via* an acylation reaction employing conditions previously developed for *N*-tosylpyrroles.²² Specifically, in the presence of excess of acetic acid, dipyrrroyl derivative **4** undergoes double acylation followed by aldol-type condensation eventually affording **1b** in 12% yield along with 9% of **6** (Scheme 2). The overall efficiency was further improved by the decrease in amounts of TFAA and TFA. In general, the developed method allows for assembling 6,12-difunctionalized DPND derivatives **1b–h** as well as cyclophane analogues **10–r** (Table 1). During our ongoing adventure with these strongly fluorescent chromophores, it appeared that DPNDs are formed only when alkyl carboxylic acids are used, although with some exceptions (**1j**, **1k**). The highest yield (32%) has been recently reported for enanthic acid ($\text{C}_6\text{H}_{13}\text{COOH}$)¹⁹ as a carboxylic partner. All attempts with carboxylic acids other than aliphatic ones failed.

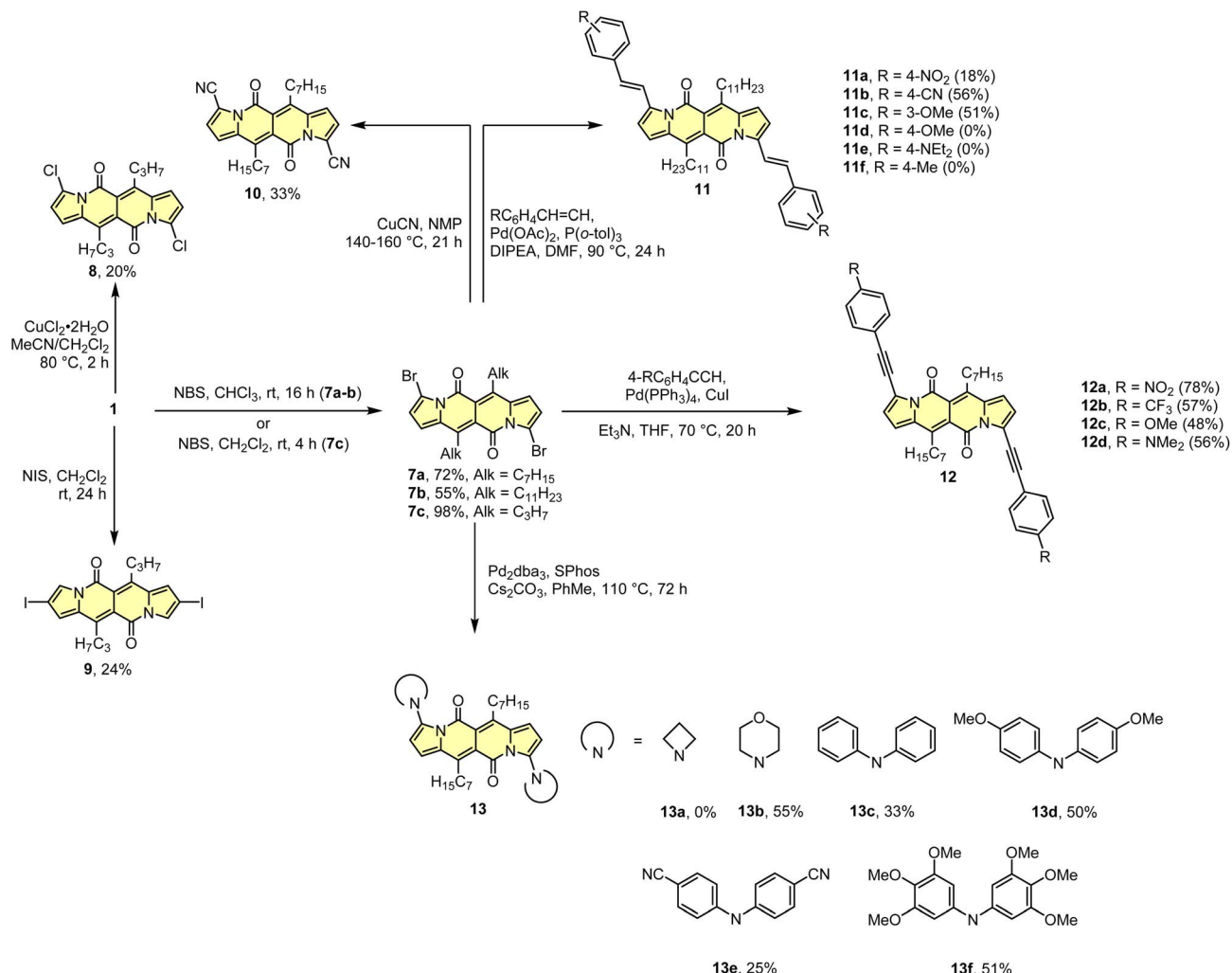
3. Synthetic modifications of the DPND core

As the DPND core consists of two flanking pyrrole rings as well as the carbonyl-based central part, synthetic modifications of this chromophore should be a result of inherent reactivity (to a certain extent) of these two parts. It should be noticed here that all three available positions within the pyrrole ring are not equivalent due to unsymmetrical mode of fusion between 5- and 6-membered rings. As a proof of concept, we initially envisaged bromination of the pyrrole part (Scheme 3) as it is well known that aromatic halides are outstanding feedstocks in a wide range of transition-metal-catalyzed cross-coupling reactions.²³

Indeed, **1** selectively undergoes double bromination reaction at the positions 3 and 9 (product **7**) using NBS (*N*-bromosuccinimide) as a bromine atom source. Moreover, we found out that chloroform stabilized with amylene performed better in this reaction compared to that one stabilized with ethanol. Besides bromination, chlorination and iodination reactions were examined by Ayitou and others.²¹ While under the influence of $\text{CuCl}_2 \cdot 2\text{H}_2\text{O}$ double chlorination reaction occurs at the positions 3 and 9 (product **8**), applying NIS (*N*-iodosuccinimide) as an iodination reagent results in completely different regioselectivity, giving rise to 2,8-diiodinated DPND (**9**). The unexpected regioselectivity of iodination was presumably ascribed to a large size of an iodine atom (potential steric clash with a carbonyl oxygen atom). However, the fact of decreased reactivity at the α position of a pyrrole ring caused by the presence of electron-withdrawing groups within this ring cannot be excluded.²⁴

The very presence of halogen atoms at positions 3 and 9 should enable further transformations. As an example, subjecting compound **7a** to the Rosenmund-von Braun reaction





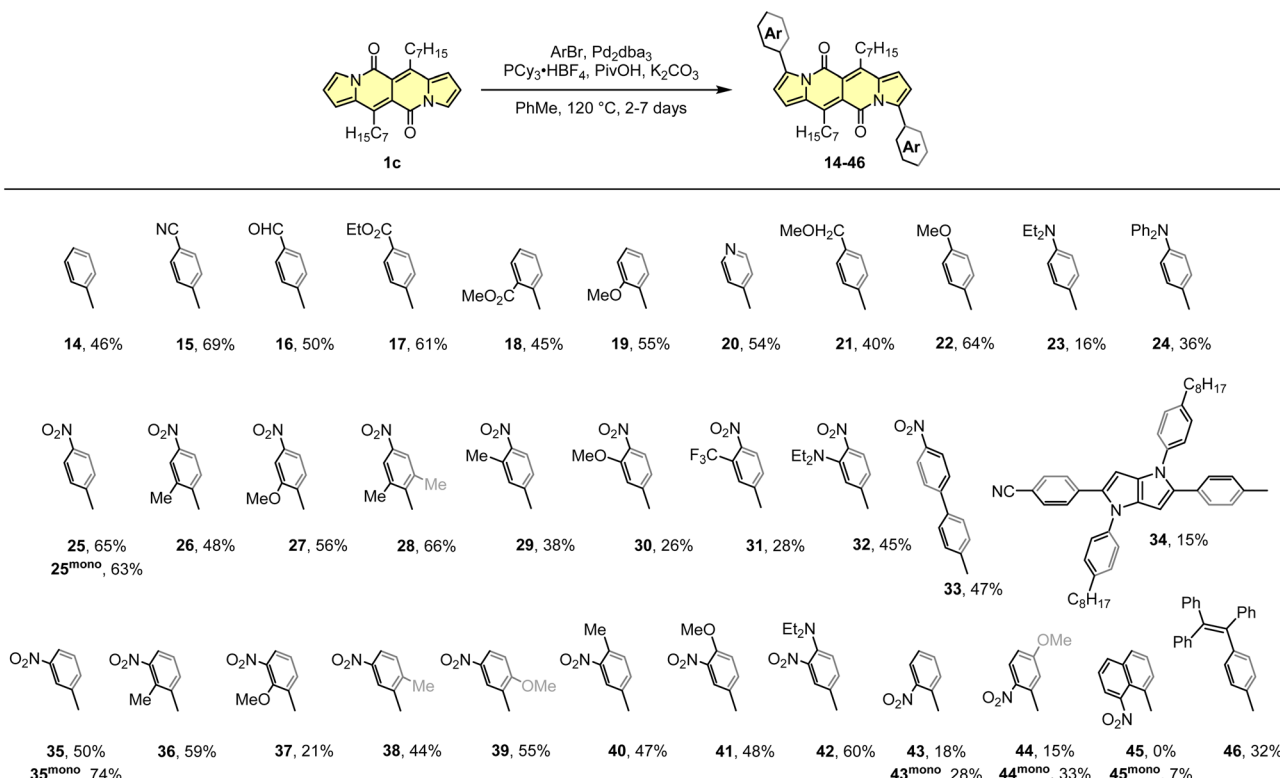
Scheme 3 Derivatization of the DPND core based on halogenation reactions.

conditions resulted in dicyano derivative **10** in 33% yield,¹⁸ proving that further derivatization of DPND-based halides is possible.

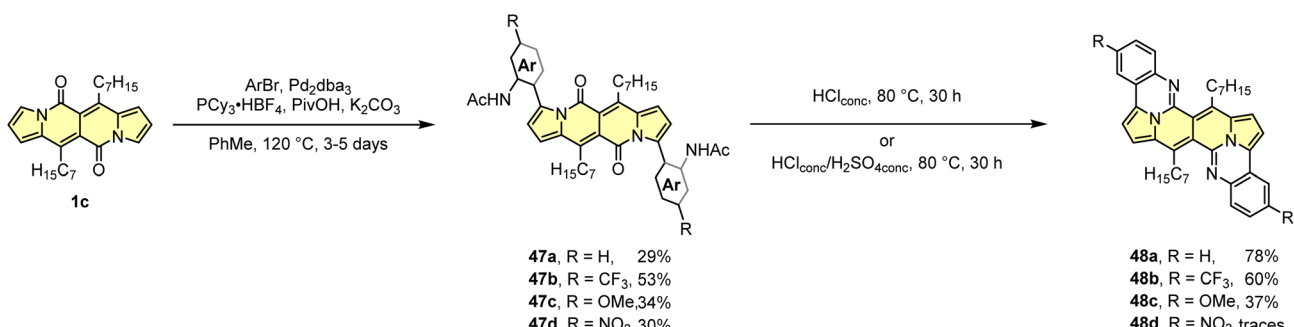
As mentioned above, halides constitute one of the best platforms for derivatization, especially towards enlarged architectures by employing acetylenes²⁵ or styrenes^{6a,26} as coupling partners. As a matter of fact, dibrominated DPNDs of type **7** were successfully transformed into a variety of π -expanded platforms employing the main types of cross-coupling reactions. The $\text{Pd}(\text{OAc})_2/\text{P}(o\text{-tol})_3$ system proved to be effective in the construction of quadrupolar, centrosymmetric molecules **11a-f** with double bond linkages *via* the Heck reaction.²⁷ Employing a typical catalytic system for the Sonogashira reaction led to molecules **12a-d** bearing triple bond π -spacers.¹⁸ Finally, amine-decorated DPNDs **13a-f** can be assembled *via* the Buchwald–Hartwig amination reaction using the $\text{Pd}_2\text{dba}_3/\text{SPhos}$ system.²⁸ It should be mentioned here that some of π -expanded derivatives, especially those bearing strongly electron-donating groups, were not sufficiently stable during isolation or it was not possible to isolate them in a pure form due to similar affinity to a stationary phase and/or lower solubility.

Compared to cross-coupling reactions of heteroaryl halides, transition-metal-catalyzed C–H activation processes are characterized by higher atom and step economy.²⁹ In other words, employing C–H activation for the functionalization of organic chromophores helps avoiding often problematic derivatization (halogenation, borylation *etc.*).

The DPND core appeared to be an ideal platform for the study on direct arylation reaction (Scheme 4)³⁰ which was widely used as a common strategy toward organic materials.³¹ The catalytic system involves Pd_2dba_3 as a catalyst, $\text{PCy}_3\text{-HBF}_4$ as a ligand, PivOH as an additive, and allows for the functionalization of the DPND core at the positions 3 and 9 with differently decorated arene rings. From the view-point of industrial research, it was proven that Pd_2dba_3 can be replaced with cost-efficient $\text{Pd}(\text{OAc})_2$.³² Variety of aryl halides are reactive towards the DPND core, nevertheless those bearing electron-withdrawing groups performed better. In a typical reaction, 2.2–3-fold excess of aryl halide was used to achieve doubly-arylated derivatives. Monoarylation is also achievable by applying 2.0 equivalents of **1c** *versus* aryl halide, as proved for some nitroaryl-decorated DPNDs (Scheme 3).^{30b} Interestingly,



Scheme 4 Direct arylation of the DPND core.



Scheme 5 Functionalization of carbonyl moieties within the DPND core.

only for 1-bromo-8-nitronaphthalene we were not able to obtain doubly arylated derivative due to high steric congestion within the reaction centre. This resulted in messy reaction outcome where the expected, doubly-functionalized product was not detected at all.

The developed direct arylation methodology was further applied in the synthesis of N-doped analogues of polycyclic aromatic hydrocarbons (PAHs) (Scheme 5).³³ Arylation of the DPND core with sterically congested aryl halides bearing acetyl amino groups led to a series of dyes 47 that can be smoothly transformed into polycyclic aromatics of type 48, under the influence of strong acid(s). Here, the reactivity of carbonyl moieties within the DPND core was tested in a condensation process, similarly to the reaction described for perylene bisimides.³⁴ Among tested derivatives, bis-arylated dye 47d failed as

a precursor of 48d presumably due to low nucleophilicity of nitrogen caused by the presence of a strongly electron-withdrawing NO₂ group at the *para* position relative to NHAc.

4. The optoelectronic properties of dipyrrolonaphthyridinedione and its applications

Unsubstituted compound **1a** exhibits an intense structured absorption band with the longest maxima ($\lambda_{\text{abs}}^{\text{max}}$) at 509 nm in dichloromethane (CH₂Cl₂), and molar extinction coefficient of 26 600 M⁻¹ cm⁻¹ (Table 2). Alkyl-substituted derivatives **1b-h** shows similar structural absorption bands that are hypsochromically-shifted compared to **1a** (Fig. 3 and Table 2),

Table 2 Photophysical properties of DPNDs measured in dichloromethane¹⁸

Dye	$\lambda_{\text{abs}}^{\text{max}} [\text{nm}]$	$\epsilon_{\text{max}} [\text{M}^{-1} \text{cm}^{-1}]$	$\lambda_{\text{em}}^{\text{max}} [\text{nm}]$	Φ_{fl}	$\delta\nu^a [\text{cm}^{-1}]$
1a	509	26 600	535	0.61 ^b	950
1b	499	29 200	523	0.66 ^b	900
1c	504	29 300	528	0.71 ^b	900
1d	505	23 100	543	0.58 ^b	1400
1e	510	28 300	536	0.26 ^b	950
1f	500	28 000	526	0.67 ^b	1000
6	503	24 600	601	0.46 ^b	3240
10	517	34 600	537	0.25 ^b	720
11a	621	60 200	699	0.016 ^c	1800
11b	610	56 300	671	0.022 ^c	1500
11c	603	55 100	662	0.041 ^c	1500
12a	599	57 300	633	0.51 ^c	900
12b	584	47 400	616	0.51 ^c	900
12c	601	52 400	643	0.59 ^c	1100
12d	645	56 600	736	0.17 ^c	1900

^a Stokes shift *i.e.* difference between lowest energy absorption band and highest energy emission band expressed in cm^{-1} . ^b Reference: Rhodamine 6G in EtOH ($\Phi_{\text{fl}} = 0.94$). ^c Reference: cresyl violet in MeOH ($\Phi_{\text{fl}} = 0.54$).

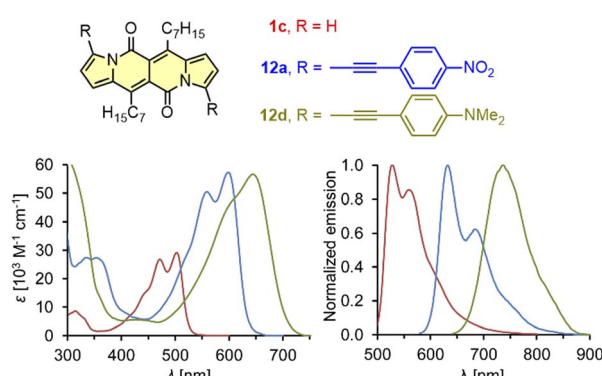


Fig. 3 Absorption and normalized emission spectra of dye **1c** (red), **12a** (blue), and **12d** (green). Adapted with permission from ref. 18 Copyright 2016 Royal Society of Chemistry.

probably due to additional steric interactions between alkyl chains at positions 6 and 12 with carbonyl groups. The origin of these “sub-bands”, although not investigated in detail for DPNDs, one may possibly attribute to vibrational progression in the excited state, as found previously for BOPHY dyes.⁷ In general, DPNDs **1a–h** are strongly fluorescent in CH_2Cl_2 (Φ_{fl} up to 0.71). Compared to BOPHYs however, DPNDs emit less intensively as values of Φ_{fl} measured for simple BOPHY-type dyes approach ≈ 0.9 .

It should be mentioned that during the preparation of alkyl-substituted DPNDs (*i.e.* **1c**), a trifluoroacetyl derivative **6** is also obtained as a minor product (Scheme 2). Here, the emission band is red-shifted by *ca.* 80 nm as compared with its analog **1c** (Table 2) and both absorption and emission bands become structureless.¹⁸ The most convenient way toward dyes that absorb and emit at significantly longer wavelengths is to

introduce arylethynyl or arylethynyl moieties at the core’s peripheries. The Sonogashira coupling of **7a** with different arylacetylenes gave rise to a series of π -expanded DPNDs **12** which generally absorb at 584–601 nm and emit at 616–643 nm (Table 2 and Fig. 3).¹⁸ Importantly, the largest red-shift of both bands was observed for **12d** bearing Et_2N auxochromes at peripheries which suggests that the DPND core as a whole behaves as an *electron acceptor*. Although the value of Φ_{fl} dropped down to 0.17 (compared with **12a–c**), **12d** absorbs in the red region of the spectrum and emits at 736 nm.

In turn, vinylidene-linked systems **11a–c**²⁷ absorb at longer wavelengths that is around 603–621 nm (Table 2) and this is due to better electronic conjugation³⁵ between the core and groups at the peripheries. These dyes are poorly emissive ($\lambda_{\text{em}}^{\text{max}} = 662$ –669 nm, $\Phi_{\text{fl}} < 0.1$), however, probably because of an additional energy dissipation mechanism, *i.e.* *E*–*Z* isomerization of a $\text{C}=\text{C}$ double bond.³⁶

An “electron-accepting” character of the DPND core was further probed by studying a variety of weakly coupled, quadrupolar dyes prepared *via* direct arylation methodology.^{30a} As expected, the presence of biaryl-type connection between the DPND core and auxochromes at peripheries leads to weaker electronic conjugation between them. The dihedral angle between the DPND core and an aryl substituent was found to be $\approx 40^\circ$ – 45° or 50° – 55° based on DFT methods^{30a} and X-ray analysis,^{30b,30c} respectively. Consequently, these dyes feature absorption and emission bands at shorter wavelengths compared to **11** and **12** (Table 3 and Fig. 4). In general, synthesized dyes are moderately fluorescent ($\Phi_{\text{fl}} \approx 0.3$ – 0.6) and the emission band is located in the red region of the spectrum ($\lambda_{\text{em}}^{\text{max}} \approx 600$ – 620 nm).

The largest change in the optical behaviour was noted for DPNDs with NR_2 groups at peripheries: bathochromically-shifted both absorption and emission bands and lower value of Φ_{fl} by contrast with **15–21** (Table 3 and Fig. 4). According to theoretical calculations (Fig. 5), compounds bearing CN, H and Me groups at peripheries feature locally-excited transitions (S_1 –LE(π – π^*)), where HOMO and LUMO wavefunctions are located mostly within the DPND core. In contrast, for NMe_2 and OMe groups the electron density is shifted from outer groups toward the core upon the photoexcitation, with largest net change noted for the dye bearing NMe_2 group.

The above-mentioned observations suggest that placing electron-donating groups at peripheries induce significant red shift of absorption and emission and the DPND core behaves like an “electron-acceptor”.

The electron-accepting character of the core was further deeply investigated²⁸ by studying a series of dyes **13a–f** decorated with an amine function connected directly with the core or by a π -spacer (**12d**, **23** and **24**). We found that these dyes feature evident solvatofluorochromic behavior (Fig. 6) that is the emission bands shift toward lower energies (usually $\lambda_{\text{em}}^{\text{max}} > 700$ nm) as well as the value of Φ_{fl} lowers as polarity of the medium increases (Table 4). Interestingly, compound **13e** exhibits slightly different behavior compared to other dyes belonging to a series **13**. The very presence of four CN groups withing amine moieties partially hampers electron density shift toward the

Table 3 Photophysical properties of DPND dyes bearing a biaryl-type bridge

Dye	R	Solvent	$\lambda_{\text{abs}}^{\text{max}} [\text{nm}]$	$\varepsilon_{\text{max}} [\text{M}^{-1} \text{ cm}^{-1}]$	$\lambda_{\text{em}}^{\text{max}} [\text{nm}]$	Φ_{fl}	$\delta\nu [\text{cm}^{-1}]$
15	4-CN	CH_2Cl_2	543	33 200	602	0.36 ^c	1800
		DMSO ^a	549	31 000	614	0.38 ^c	1900
16	4-CHO	CH_2Cl_2	547	37 100	607	0.36 ^c	1800
		DMSO ^a	555	36 600	619	0.36 ^c	1900
17	4-CO ₂ Et	CH_2Cl_2	544	34 000	600	0.44 ^c	1700
		DMSO ^a	550	27 200	614	0.40 ^c	1900
18	2-CO ₂ Me	CH_2Cl_2	536	31 400	581	0.63 ^c	1400
		DMSO ^a	542	32 100	591	0.57 ^c	1500
19	2-OMe	CH_2Cl_2	536	31 100	603	0.60 ^c	2100
		DMSO ^a	541	30 200	607	0.54 ^c	2100
20	4-Pyridyl ^e	CH_2Cl_2	535	31 600	582	0.46 ^c	1500
		DMSO ^a	540	31 800	599	0.45 ^c	1900
21	4-CH ₂ OMe	CH_2Cl_2	542	37 100	601	0.38 ^c	1800
		DMSO ^a	555	27 100	620	0.42 ^c	1900
22	4-OMe	CH_2Cl_2	550	26 600	624	0.43 ^c	2100
		DMSO ^a	557	34 800	643	0.36 ^c	2400
23	4-NEt ₂	CH_2Cl_2	615	39 500	735	0.10 ^d	2700
24	4-NPh ₂	CH_2Cl_2	583	38 000	— ^b	— ^b	— ^b
25	4-NO ₂	CH_2Cl_2	548	29 300	611	0.46 ^c	1900
34	Pyrrolo[3,2- <i>b</i>]pyrrole core	CH_2Cl_2	399, 579	83 600, 47 300	— ^b	— ^b	— ^b
43	2-NO ₂	CH_2Cl_2	538	26 500	— ^b	— ^b	— ^b
		DMSO ^a	545	26 800	— ^b	— ^b	— ^b

^a Solutions were sonicated for 15–30 min directly before measurement. ^b Not measured due to low S/N ratio. ^c Sulforhodamine 101 was used as a reference ($\Phi_{\text{fl}} = 0.95$ in EtOH). ^d Cresyl violet was used as a reference ($\Phi_{\text{fl}} = 0.54$ in MeOH). ^e 4-Pyridyl groups are attached to the DPND core instead of R-C₆H₄.

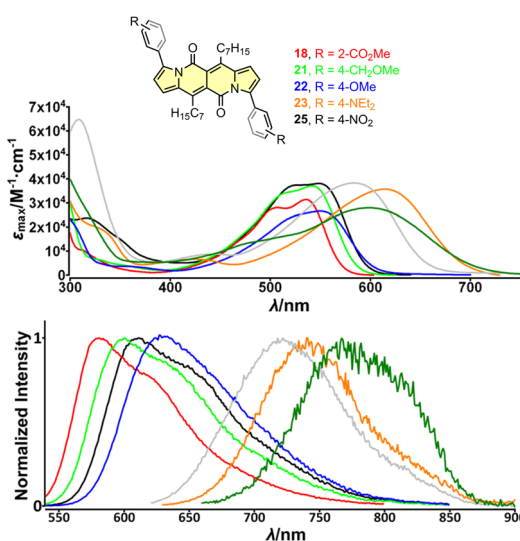


Fig. 4 Top: absorption spectra of compounds **18** (red), **21** (green), **22** (blue), **23** (orange) and **25** (black) measured in dichloromethane. Bottom: normalized emission spectra of compounds **18** (red), **21** (green), **22** (blue), **23** (orange) and **25** (black) measured in dichloromethane. Adapted with permission from ref. 30a. Copyright 2018 Wiley.

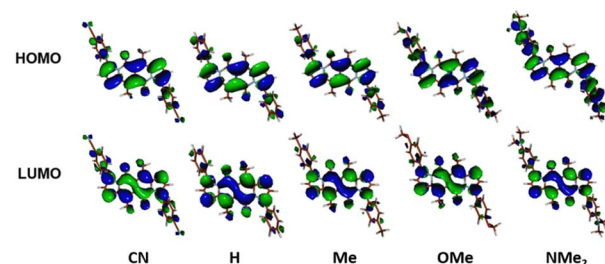


Fig. 5 Frontier molecular orbitals of compounds from DPND(C₆H₄R)₂ series calculated in C₂ symmetry at the DFT(B3-LYP) methods using the cc-pVQZ basis set. Adapted with permission from ref. 30a. Copyright 2018 Wiley.

DPND core and hence the efficient formation of dark charge-transfer (CT) states which results in less pronounced solvatofluorochromism. On the other hand, Φ_{fl} increases sharply in more polar environment reaching values of 0.4–0.6 (Table 4).

Cyclic voltammetry (CV) appeared to be an excellent methodology to probe the electronic structure of dipyrrolonaphthiridinediones (DPNDs) (Fig. 7–9). A CV trace of unsubstituted dye **1a** displays irreversible oxidation/reduction events and the shape of the CV curve changes with a rising number of redox cycles (Fig. 7).¹⁸ Upon an oxidation event a black, insoluble deposit



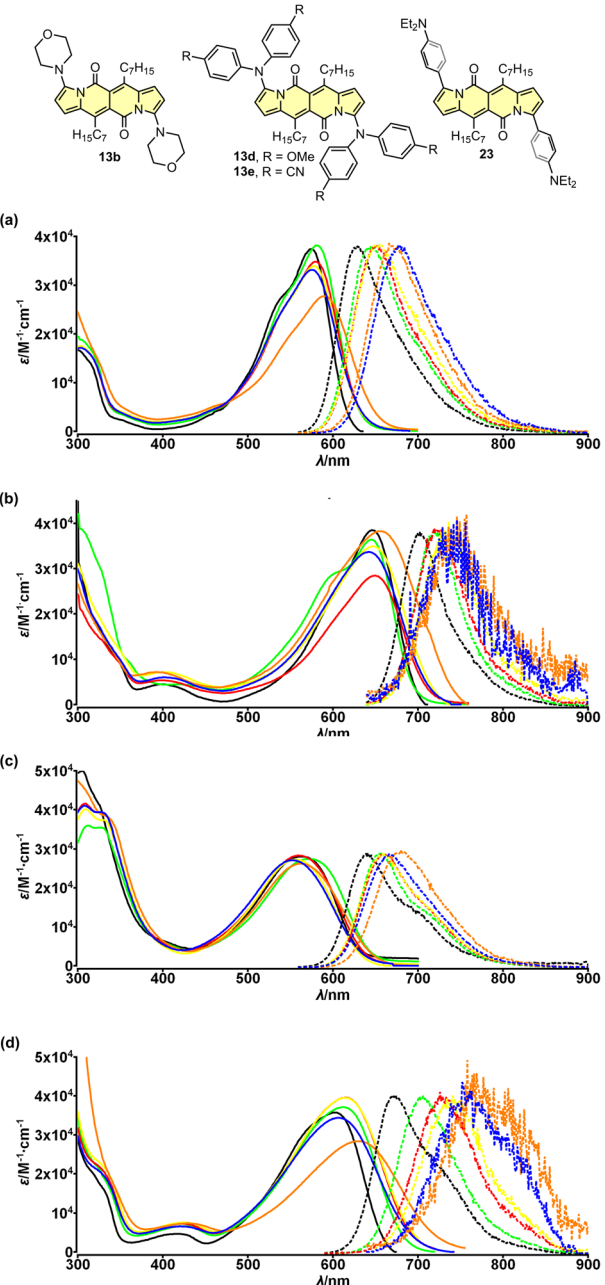


Fig. 6 Absorption (solid) and emission (dotted) spectra of compounds **13b** (a), **13d** (b), **13e** (c) and **23** (d) measured in cyclohexane (black), toluene (green), THF (red), CH_2Cl_2 (yellow), MeCN (blue) and DMSO (orange). Adapted with permission from ref. 28 Copyright 2018 American Chemical Society.

appeared on an anode which did not dissolve upon reduction. Such a deposit did not form in the case of **1c**, **10** and **12b** (Fig. 8). For **1c**, the results show a reversible reduction with $E_{1/2} = -1.125 \text{ V vs. SCE}$ ($E_{\text{LUMO}} = -3.2 \text{ eV}$) in the accessible potential range. The appearance of reducible CN groups in the chromophore structure (compound **10**, Fig. 8) results in an additional reduction wave within the CV curve ($E_{1/2} = -0.675 \text{ V vs. SCE}$) that can be clearly connected with those groups, while the often reversible reduction event characteristic for the DPND core

shifted toward more negative potentials ($E_{1/2} = -1.215 \text{ V vs. SCE}$) and the oxidation wave is not present in the accessible potential range. This constitutes a general feature for DPND derivatives bearing electron-withdrawing groups at the peripheries.^{30a,b} When it comes to electrochemically-driven oxidation events, most of DPND derivatives show irreversible oxidation wave (if any). The situation is changed when another, easily oxidizable groups are present in the structure (Fig. 9).²⁸ Cyclic voltammograms of electron-rich DPND derivatives containing NR_2 groups (i.e. **13f**, Fig. 9), beside one reversible reduction event associated with the core, frequently include two oxidation waves where the first event is connected with a reversible (often stepwise) oxidation of the $-\text{NR}_2$ auxochrome while the second one (irreversible) comes from an oxidation process within the core.

Although highly-emissive in a solution, simple DPNDs i.e. **1c**^{30c} or **1h**^{8d} do exhibit weak fluorescence in the solid state, as these molecules mostly form H-aggregates in a crystalline state (Fig. 16, *vide infra*). The tetraphenylethylene moiety (TPE) seemed to be an ideal platform for inducing emission in the solid state,³⁷ thus we investigated emission properties both in the solid and aggregated states for the quadrupolar dye **46** bearing two TPE units.^{30c} Beside red-shifted absorption and emission in a CH_2Cl_2 solution as compared with **1c** (Table 2) and **14** (Table 5), **46** emits weakly in the solid state with $\lambda_{\text{em}}^{\text{max}} = 659 \text{ nm}$ and $\Phi_{\text{fl}} = 0.12$ (Table 5). Fluorescence properties in the aggregated state were studied in THF/water mixtures (Fig. 10). DPND **1c** showed aggregation-caused quenching effect (ACQ) as fluorescence intensity measured at 523 nm lowered at water fractions equal or higher than 80%. In turn, **46** undergoes aggregation at lower water proportions probably due to increased hydrophobicity, and then modest jump in the emission intensity was observed at water contents from 70 to 80%, possibly related to aggregation effects (aggregation-induced emission (AIE)). It means that for **46** both ACQ (dominant) and AIE (weak) effects can be observed. Direct comparison between **46** and its simple analogue **14** reveals almost no enhancement in solid state emission (Table 5). Moreover, we performed DFT calculations for some pairs of DPND molecules extracted from respective X-ray crystal structures. For most of pairs, very low or zero oscillator strengths were determined for $S_1 \rightarrow S_0$ transitions.^{30c} Additionally, some of them manifested CT character. In this work we proved somehow that the TPE moiety is not a magic group that always induces emission in the solid/aggregated state, but appearance of such feature depends only on which mode of crystal lattice arrangement is dominant (H- or J-aggregates).

Probing reactivity of $\text{C}=\text{O}$ moieties, we successfully designed and synthesized N-doped analogues of polycyclic aromatic hydrocarbons (PAHs) (**48**) starting from the DPND core (Fig. 11a and Table 6).³³ These propeller-shaped dyes are intensively blue in a solution while having extremely weak emission ($\Phi_{\text{fl}} < 0.001$, Table 6 and Fig. 11b). Based on transient-absorption measurements we concluded that the first singlet excited state of these dyes tend to deexcite *via* internal conversion rather than fluorescence or triplet state formation. A moderate red-shift of both bands can be observed when OMe group is present in the chromophore structure (**48a** vs. **48b**,

Table 4 Photophysical properties of amine-decorated DPNs in different solvents²⁸

Dye	Solvent	$\lambda_{\text{abs}}^{\text{max}} [\text{nm}]$	$\epsilon_{\text{max}} [\text{M}^{-1} \text{cm}^{-1}]$	$\lambda_{\text{em}}^{\text{max}} [\text{nm}]$	Φ_{fl}	$\delta\nu^a [\text{cm}^{-1}]$
13b	Cyclohexane	575	37 000	628	0.35 ^b	1500
	Toluene	582	38 000	645	0.32 ^b	1700
	THF	580	35 000	650	0.35 ^b	1900
	CH ₂ Cl ₂	578	34 000	653	0.27 ^b	2000
	MeCN	576	29 000	659	0.21 ^b	2200
	DMSO	590	28 000	670	0.18 ^b	2000
13d	Cyclohexane	645	38 000	702	0.39 ^c	1300
	Toluene	654	35 000	718	0.26 ^c	1400
	THF	648	37 000	720	0.10 ^c	1500
	CH ₂ Cl ₂	648	35 000	727	0.07 ^c	1700
	MeCN	642	34 000	732	0.01 ^c	1900
	DMSO	656	38 000	739	0.01 ^c	1700
13e	Cyclohexane	565	nd	639	0.37 ^b	2000
	Toluene	571	27 000	655	0.49 ^b	2200
	THF	560	28 000	658	0.62 ^b	2700
	CH ₂ Cl ₂	558	27 000	659	0.61 ^b	2700
	MeCN	554	27 000	666	0.63 ^b	3000
	DMSO	564	26 000	677	0.47 ^b	3000
23	Cyclohexane	603	36 000	670	0.40 ^c	1700
	Toluene	613	37 000	702	0.25 ^c	2100
	THF	615	40 000	729	0.11 ^c	2500
	CH ₂ Cl ₂	615	39 000	735	0.10 ^c	2700
	MeCN	607	34 000	750	0.02 ^c	3100
	DMSO	631	28 000	758	0.02 ^c	2700

^a Stokes shift *i.e.* difference between lowest energy absorption band and highest energy emission band expressed in cm^{-1} . ^b Sulforhodamine 101 was used as a reference ($\Phi_{\text{fl}} = 0.95$ in EtOH). ^c Cresyl violet was used as a reference ($\Phi_{\text{fl}} = 0.54$ in MeOH).

Table 6). Due to the presence of basic nitrogen atoms, **48a** was found to be acid-responsive (Fig. 11c–e). Namely, adding an increasing amount of trifluoroacetic acid (TFA) to a solution of **48a** in CH₂Cl₂ results in two new absorption bands centered at 467 nm and 776 nm, while the main absorption band of pure **48a** vanished substantially. Broad nature of the longer-wavelength absorption band suggests that mainly monoprotonation took place and the resulted molecule features internal

donor–acceptor (D–A) character. Double protonation can be achieved by employing stronger acid – methanesulphonic acid (MsOH) (Fig. 11d). First of all, significantly smaller amount of acid is needed for monoprotonation to occur as compared with TFA (10 eq. *vs.* 416 eq., respectively). Similarly to TFA, upon adding 10 eq. of MsOH, a new, broad absorption band appeared around 776 nm. Higher excess of MsOH (10 eq. \rightarrow 250 eq.) led to complete disappearance of a broad band above 700 nm and

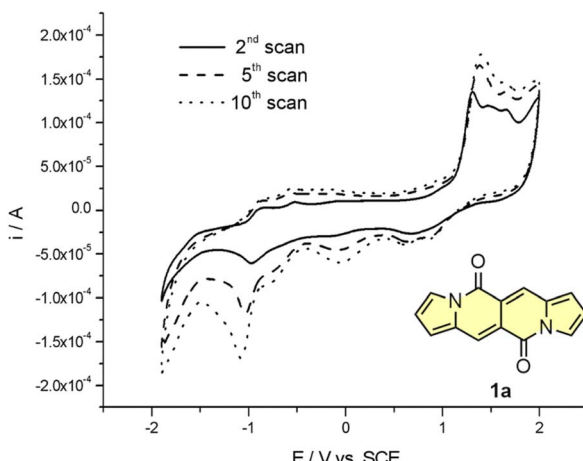


Fig. 7 Cyclovoltammetric curve registered for **1a** in dichloromethane in the entire range of examined potentials: $-1800 \div 2100 \text{ mV}$, $v = 100 \text{ mV s}^{-1}$. Adapted with permission from ref. 18 Copyright 2016 Royal Society of Chemistry.

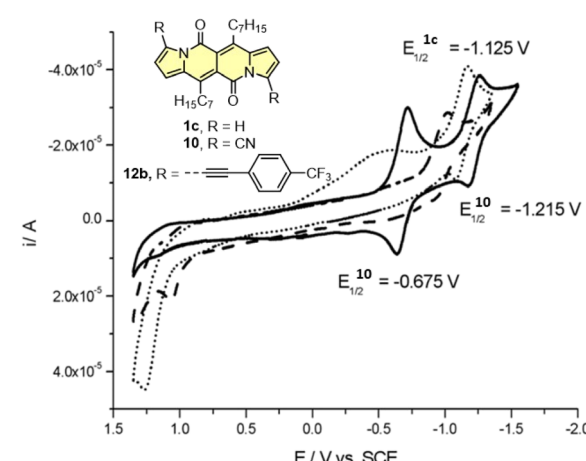


Fig. 8 Cyclovoltammograms of the dyes **1c** (dotted line), **10** (solid line) and **12b** (dashed line) in dichloromethane measured using the saturated calomel electrode (SCE) as the reference. Adapted with permission from ref. 18 Copyright 2016 Royal Society of Chemistry.



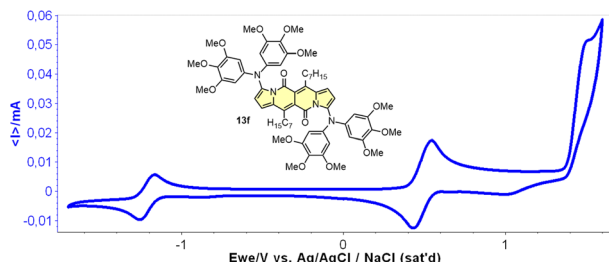


Fig. 9 A cyclovoltammogram of dye **13f** in dichloromethane measured using Ag/AgCl/NaCl as the reference. Adapted with permission from ref. 28 Copyright 2018 American Chemical Society.

a new absorption band emerged at 675 nm confirming stepwise double protonation of **48a**. Both protonation processes are completely reversible as by adding excess of triethylamine (Et_3N) the absorption spectrum as well as the color of **48a** can be fully recovered (Fig. 11e).

In all of the above-described chromophores, a geometry of the core was influenced only by the presence of substituents at positions 6 and 12 as well as vicinity of substituents at positions 3 and 9 (an α position within a pyrrole ring). DFT calculations for some arylated DPNDs revealed that the expected deviation from the core plane mainly caused by the presence of arene rings at position 3 and 9 should be no greater than 8° .^{30a} In order to test how high distortion influences of the photophysical aspects, we assembled three analogues of cyclophanes based on the DPND core (**10-r**)²⁰ that differ in a length of an alkane bridge. X-ray analysis of **1p** revealed that the distortion from the planarity reaches 28° (Fig. 12).

DFT calculation supported the obtained degree of distortion (Table 7). Interestingly, chromophore **1o** (C_7 bridge) tends to increase its distortion degree upon photoexcitation while other cyclophane analogues as well as its open analogue **1o**^{open}

Table 5 Photophysical properties of DPND dyes **14** and **46** in CH_2Cl_2 solution and in a solid state

Dye	$\lambda_{\text{abs}}^{\text{max}}$ [nm]	ϵ_{max} [$\text{M}^{-1} \text{cm}^{-1}$]	$\lambda_{\text{em}}^{\text{max}}$ [nm]	Φ_{fl}^a	$\delta\nu$ [cm^{-1}]
14	CH_2Cl_2 536	24 000	599	0.71	2000
	Solid	562	601	0.15	1200
46	CH_2Cl_2 553	29 000	644	0.42	2600
	Solid	574	659	0.12	2200

^a Determined using a spectrofluorimeter equipped with a calibrated integrating sphere.

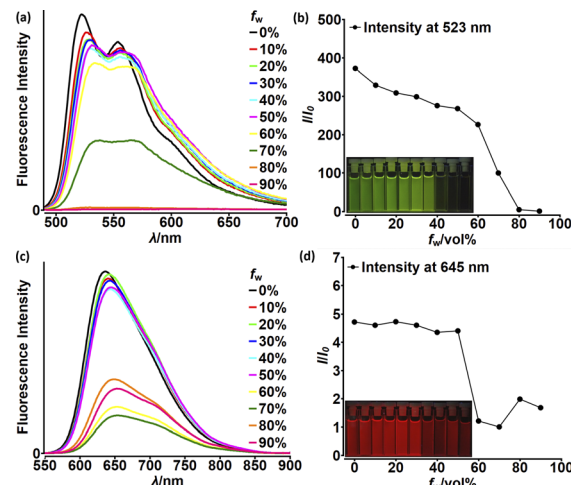


Fig. 10 Fluorescence spectra of **1c** (a) and **46** (c) in THF–water mixtures of different relative proportions. Plots of maximum intensity vs. % water fraction (f_w) for dyes **1c** (b) and **46** (d). Insets: photographs of **1c** (b) and **46** (d) in THF–water mixtures with different water fractions under UV illumination (0% to 90% water fraction from left to right). Dye concentration: ~ 10 mM. Adapted with permission from ref. 30c. Copyright 2018 Royal Society of Chemistry.

feature lower value of a distortion angle (Table 7). In general, **1o-r** absorb at shorter wavelengths than **1c**, but the most significant difference between an “open dye” and cyclophanes lies in their luminescence (Table 8). Namely, while emission bands determined for **1p-r** are red-shifted by 30–40 nm as compared with **1c**, in the case of **1o** the emission band is located above 600 nm that is in the red region of the spectrum and particularly low values of Φ_{fl} were determined. In terms of emission intensity, **1p-r** behave similarly to **1c** ($\Phi_{\text{fl}} = 0.40$ –0.55), however emission bands are located at lower energies. Transient-absorption studies performed for cyclophane analogues suggested that presumably efficient formation of triplet state is responsible for distinct emission properties of **1p**.

Dipyrrolonaphthyridinediones versus other cross-conjugated chromophores

Although cross-conjugated, the DPND core is different from well-known dyes of this type such as isoindigo (**II**),³⁸ diketopyrrolopyrrole,³⁹ or cibalakrot⁴² (Fig. 13) as it contains a “pure” pyrrole ring as an electron-donating moiety. This factor directly translates into particularly distinct one-photon optoelectronic behavior compared with other cross-conjugated structures (Table 9 and Fig. 13). According to the data collected in Table 9, among all dyes **B-II-B** is weakly- or non-fluorescent,⁴⁰ features the lowest molar absorption coefficient (ϵ_{max}) and absorbs at shorter wavelength ($\lambda_{\text{abs}}^{\text{max}} = 517$ nm) than **14**. Compound **14** emits light with $\Phi_{\text{fl}} = 0.71$ with a maximum noted at $\lambda_{\text{em}}^{\text{max}} = 599$ nm that is most red-shifted compared with other cross-conjugated chromophores, although **Ph-DPP-Ph** has a larger value of Stokes' shift.

Direct comparison of electrochemically-derived energetic levels may be useful from the view-point of optoelectronics

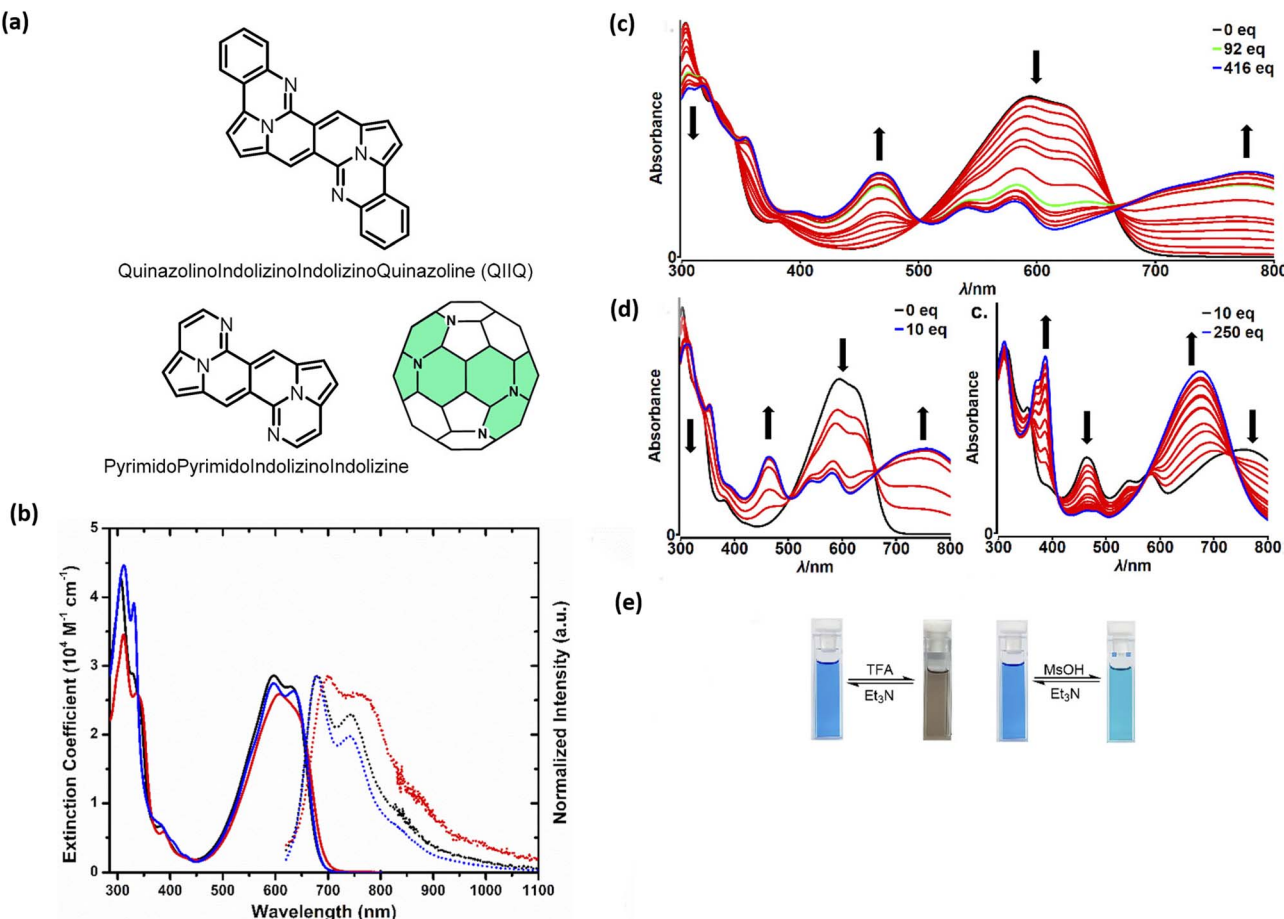


Fig. 11 (a) General structure of the QIIQ skeleton; (b) absorption (solid) and emission (dotted) spectra of **48a** (black), **48b** (red), and **48c** (blue) in toluene. Emission spectra from 570 nm excitation; (c) changes in the absorption spectra and color of **48a** in CH_2Cl_2 (2.8×10^{-5} M) upon addition of MsOH (0–10 equiv.); (d) changes in the absorption spectra and color of **48a** in CH_2Cl_2 (2.8×10^{-5} M) upon addition of MsOH (10–250 equiv.); (e) Photo of cuvettes containing **48a** in CH_2Cl_2 solution before and after addition of a large excess of TFA (left) and MsOH (right). Adapted with permission from ref. 33. Copyright 2020 American Chemical Society.

Table 6 Photophysical properties of N-doped analogues of PAHs derived from the DPND core³³

Dye	$\lambda_{\text{abs}}^{\text{max}}$ [nm]	ϵ_{max} [$\text{M}^{-1} \text{cm}^{-1}$]	$\lambda_{\text{em}}^{\text{max}}$ [nm]	Φ_{fl}	$\delta\nu$ [cm^{-1}]
48a	596	29 000	679	0.00083 ^a	2050
48b	608	26 000	704	0.00018 ^a	2240
48c	597	27 000	678	0.0023 ^a	2000

^a The fluorescence quantum yield (Φ_{fl}) of **48c** in toluene was obtained using Nile Blue ($\Phi_{\text{fl}} = 0.271$ in ethanol) as a standard and corrected for refractive index differences of the solvents. Compound **48c** was chosen as it is the most emissive, and Φ_{fl} of **48a** and **48b** were then referenced to **48c**.

(Fig. 13). DPND **14** is the most susceptible to oxidation as its E_{HOMO} level lies higher in energy than those noted for other cross-conjugated chromophores. When it comes to E_{LUMO} levels, **14** features a similar value to **Ph-DPP-Ph** and at even lower energies than that of **Ph-II-Ph** which are both considered as electron-acceptors in dyes tested toward organic electronics.

DPNDs as singlet-fission (SF) materials

The singlet fission (SF) is a process in which a higher-energy singlet exciton, typically generated by the absorption of a photon, is converted into two lower-energy triplet excitons.⁴¹

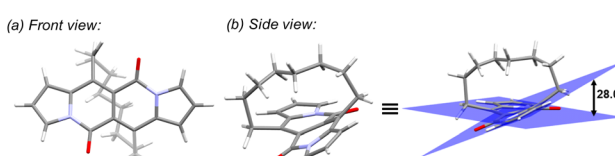


Fig. 12 Single crystal structure of **1p** (CCDC 2125168). Adapted with permission from ref. 20. Copyright 2022 Royal Society of Chemistry.

Table 7 Deviation from planarity for DPND dyes determined theoretically in the ground (S_0) and first excited state (S_1)^{20 a}

Dye	$\phi (S_0)^a$	$\phi (S_1)^a$	SE/kcal mol ⁻¹
1o^{open}	7.4°	5.6°	0
1o	32.8°	43.6°	31.2 (27.8 ^c)
1p	27.8° (28.0 ^b)	25.6°	13.6 (18.0 ^c)
1r	15.4°	12.8°	8.2 (12.2 ^c)

^a ϕ - deviation from planarity. ^b Determined based on X-ray crystallography of **1p**. ^c Determined using DFT/B3-LYP level of theory. SE - strain energy computed at MP2/cc-pVDZ level of theory.

This phenomenon features the potential to enhance the efficiency of solar cells⁴² and other optoelectronic devices as it seems to be an attractive solution to overcome Shockley-Queisser limit.⁴³ Taking a lesson from cibalakrot analogues, Wang and co-workers have investigated^{8d} the possibility of using **1h** as a potential SF material. First of all, the authors found that **1h** exhibits phosphorescence at 1019 and 1034 nm

Table 8 Photophysical properties of DPNDs **1c** and **1o–r** measured in different solvents²⁰

Dye	Solvent	λ_{abs}^a [nm]	λ_{em}^b [nm]	Φ_{fl}^c	$\Delta\nu$ [cm ⁻¹]
1c	PhMe	472, 506	526, 560	0.66	750
	THF	470, 502	524, 558	0.57	800
	C ₆ H ₅ CN	476, 508	531, 564	0.65	850
	MeCN	469, 499	527, 557	0.54	1100
1o	PhMe	492	618	0.06	4100
	THF	488	616	0.04	4300
	C ₆ H ₅ CN	493	625	0.04	4300
	MeCN	487	623	0.02	4500
1p	PhMe	483, 507	552, 577	0.55	2600
	THF	482, 503	573, 553	0.41	3300
	C ₆ H ₅ CN	489, 507	562, 581	0.40	3200
	MeCN	481	577	0.32	3500
1r	PhMe	479, 507	543, 572	0.57	2500
	THF	478, 505	542, 572	0.48	2500
	C ₆ H ₅ CN	483, 509	551, 576	0.52	2600
	MeCN	477, 500	572, 550	0.40	3500

^a Absorption maximum (bold) and shoulder. ^b Fluorescence maximum (bold) and shoulder. ^c Relative Φ_{fl} were obtained using Rhodamine 6G in ethanol ($\Phi_{\text{PL}} = 0.95$, $\lambda_{\text{exc}} = 480$ nm) as a reference.

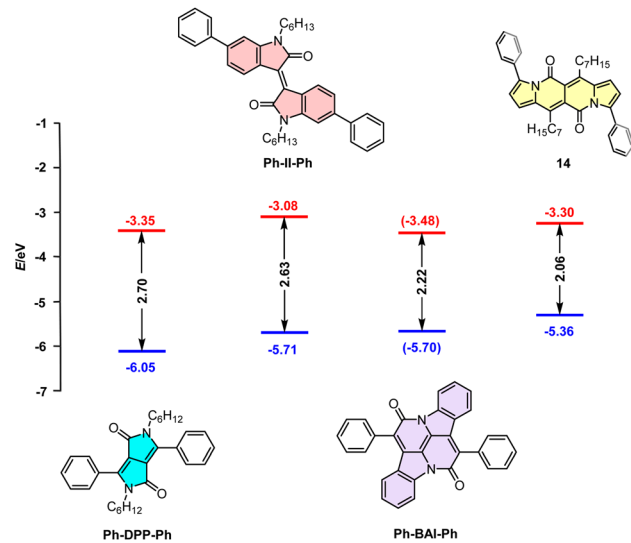


Fig. 13 Correlation diagram of the HOMOs and LUMOs of three representative cross-conjugated units and a DPND derivative **14** determined by cyclic voltammetry (CV) measurements in CH₂Cl₂ (the values in parentheses were determined using DFT calculations due to lack of the experimental data).

both in a solution and aggregated state, respectively (Fig. 14), while fluoresces weakly in the aggregated state. This result suggests that under slightly endothermic energetic conditions, a SF process can occur in polycrystalline film of **1h** that outcompetes other energy dissipation channels suggesting strong intermolecular coupling between molecules in the solid state. The authors proved that the SF process takes place in **1h** with up to 173% triplet yield and its film exhibits excellent stability upon exposure to air and light compared with pentalene⁴⁴ or cibalakrot analogues (Fig. 15).

In their follow-up work, the authors investigated¹⁹ in detail effect of molecular aggregation on SF dynamics. Specifically, the DPND molecule described above contains two longer alkyl chains (**1h** - **DPND6** in Fig. 16) which directly influences molecular arrangement in the crystal lattice with specific values of π - π distance, transverse and longitudinal offsets as well as a slipping angle (Fig. 16). In turn, compound **1a** (**DPND**) crystallizes in a nearly cofacial pattern of packing arrangement with the smaller values of transverse and longitudinal offsets, π - π distance, and a slipping angle of 66°. Here, the formation of face-to-face dimers results in stronger coupling of molecules in the crystal lattice thus an accelerated singlet fission (SF) process was eventually observed. This result may help in the future to design more efficient SF materials.

Recently, Wu and others have presented new insights into the SF mechanism by studying time-resolved spectroscopy as a function of temperature for **10**.⁴⁶ Here, the applied kinetic model developed based on the measurements and calculations includes initial conversion of S_1 state to $^1(T_1T_1)$ state followed by thermally-activated at room temperature dissociation of $^1(T_1T_1)$ into two T_1 states (Fig. 17). The yield of T_1 states formation was determined as 154%.

Table 9 Comparison of absorption and emission properties of selected dyes bearing cross-conjugated structure

Dye	Solvent	$\lambda_{\text{abs}}^{\text{max}} [\text{nm}]$	$\epsilon_{\text{max}} [\text{M}^{-1} \text{cm}^{-1}]$	$\lambda_{\text{em}}^{\text{max}} [\text{nm}]$	Φ_{fl}	$\delta\nu [\text{cm}^{-1}]$	Ref.
Ph-DPP-Ph	PhMe	480	12 600	535, 575	0.85	3400	39
Ph-II-Ph	PhMe	517	10 700	—	<0.1	—	38
Ph-BAI-Ph	PhMe	552	~33 000 ^a	575	0.77	720	12
14	CH ₂ Cl ₂	536	24 000	599	0.71	2000	30c

^a Estimated from Fig. 3 in ref. 12.

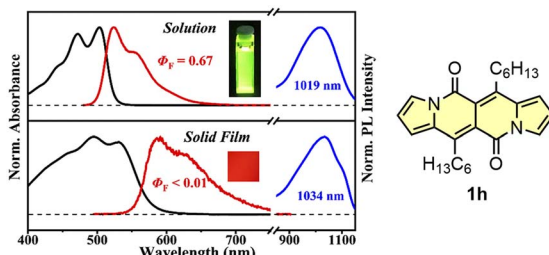


Fig. 14 Normalized absorption (black) and fluorescence (red) spectra of DPND in CH₂Cl₂ solution (10⁻⁵ M) and solid thin film (100 nm), as well as sensitized phosphorescence spectra (blue) of **1h** in polystyrene (PS) matrix (DPND : PTPBP : PS = 1 : 5 : 94) and doped thin film (DPND : PTPBP = 95 : 5). Inset: sample photographs of solution and thin film under 365 nm UV light. Adapted with permission from ref. 8d. Copyright 2020 American Chemical Society.

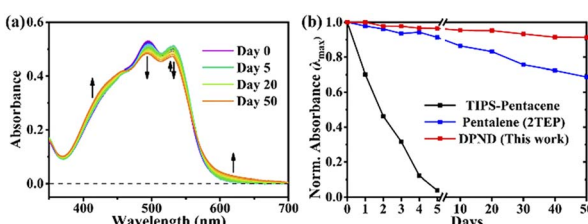


Fig. 15 Stability testing of **1h** molecule: (a) steady-state absorption spectra and (b) normalized intensity of the λ_{max} of thin films exposed to air and light. Adapted with permission from ref. 8d. Copyright 2020 American Chemical Society.

Fluorescent nitroaromatics

Nitroaromatics fluoresce occasionally as numerous possible energy dissipation channels are activated after the excitation.⁴⁷ The NO₂ auxochrome is one of the strongest electron-withdrawing moieties which ideally should improve stability and performance of NO₂-containing materials. However, the introduction of this group into the chromophore structure often results in weak emission. Although the literature outlines some strategies for enhancing emission properties of nitroaromatics,^{47a} there are still no general rules how to make nitroaromatics glow. To gain more insight into the processes that are responsible for energy dissipation in nitroaromatics, we have studied a number of these molecules where the DPND core was chosen as a reference chromophore (Table 10, Fig. 18–20).^{30b,48} The introduction of the nitro groups at the peripheries

undoubtedly implies emission intensity loss (from 0.71 for **14** to 0.41 for **25** in CH₂Cl₂), however **25** still fluoresces in the red region of the spectrum featuring red-shifted both absorption and emission bands. This initial result set the stage for the comprehensive study on fluorescence of nitroaromatics bearing the DPND core.

In general, two structural factors play a decisive role in governing emission intensity: (1) the position of NO₂ group relative to the core and (2) the substitution pattern of flanking aryl rings (Table 10, Fig. 18). Regarding the first factor, both *para*- and *meta*-NO₂-substituted derivatives are fluorescent and emission intensity lowers with the increase in solvent polarity, suggesting that a dark, charge-transfer-type (CT-type) state may be involved in energy dissipation. In contrast, close proximity of the nitro group (43–45, Scheme 4) results in weak fluorescence response (*ortho*- or *peri*-NO₂-substituted molecules) in all tested solvents.

Secondly, the introduction of additional substituents (Me, OMe, NEt₂) within flanking arene rings also contribute

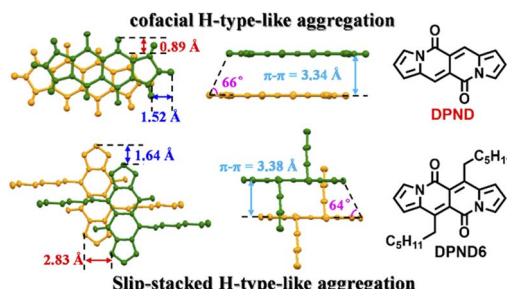


Fig. 16 Molecular arrangement of **1a** and **1h** in the solid state. Adapted with permission from ref. 19. Copyright 2021 American Chemical Society.

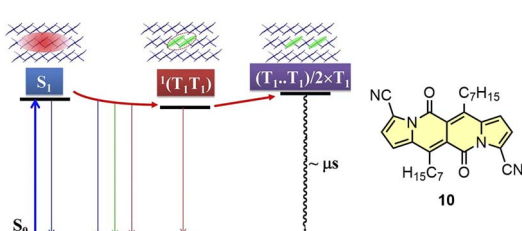


Fig. 17 Kinetic model of the SF process determined for **10**. Adapted with permission from ref. 46. Copyright 2021 American Chemical Society.



Table 10 Optical properties of nitro-decorated DPNDs

Dye	Solvent	λ_{abs} [nm]	λ_{em} [nm]	Φ_{fl}	$\Delta\nu$ [cm ⁻¹]
25	<i>o</i> -C ₆ H ₄ Cl ₂	569	605	0.45	1050
	CH ₂ Cl ₂	562	601	0.41	1150
	MeCN	559	599	0.07	1190
25 ^{mono}	<i>o</i> -C ₆ H ₄ Cl ₂	539	571	0.76	1050
	CH ₂ Cl ₂	534	568	0.36	1110
	MeCN	529	570	0.006	1370
26	<i>o</i> -C ₆ H ₄ Cl ₂	536	580	0.61	1410
	CH ₂ Cl ₂	533	578	0.49	1460
	MeCN	529	579	0.013	1630
27	<i>o</i> -C ₆ H ₄ Cl ₂	547	612	0.46	1940
	CH ₂ Cl ₂	543	610	0.21	2040
	MeCN	542	604	0.005	1910
28	<i>o</i> -C ₆ H ₄ Cl ₂	524	560	0.96	1230
	CH ₂ Cl ₂	521	560	0.34	1340
	MeCN	518	564	0.005	1570
29	<i>o</i> -C ₆ H ₄ Cl ₂	557	607	0.58	1480
	CH ₂ Cl ₂	549	605	0.45	1690
	MeCN	545	608	0.24	1900
30	<i>o</i> -C ₆ H ₄ Cl ₂	556	606	0.58	1480
	CH ₂ Cl ₂	549	604	0.44	1660
	MeCN	546	603	0.31	1890
31	<i>o</i> -C ₆ H ₄ Cl ₂	558	606	0.45	1400
	CH ₂ Cl ₂	548	602	0.31	1640
	MeCN	543	606	0.005	1940
32	<i>o</i> -C ₆ H ₄ Cl ₂	555	602	0.006	1390
	CH ₂ Cl ₂	549	608	0.003	1760
	MeCN	542	584	0.003	1330
33	<i>o</i> -C ₆ H ₄ Cl ₂	563	618	0.38	1580
	CH ₂ Cl ₂	555	615	0.28	1760
	MeCN	550	608	0.05	1730
35	<i>o</i> -C ₆ H ₄ Cl ₂	551	582	0.49	970
	CH ₂ Cl ₂	544	577	0.28	1050
	MeCN	541	575	0.04	1090
35 ^{mono}	<i>o</i> -C ₆ H ₄ Cl ₂	529	555	0.62	870
	CH ₂ Cl ₂	524	551	0.09	940
	MeCN	520	548	0.02	1000
36	<i>o</i> -C ₆ H ₄ Cl ₂	527	558	0.95	1050
	CH ₂ Cl ₂	523	555	0.92	1100
	MeCN	521	553	0.43	1110
37	<i>o</i> -C ₆ H ₄ Cl ₂	532	583	0.61	1640
	CH ₂ Cl ₂	525	584	0.52	1920
	MeCN	524	582	0.12	1900
38	<i>o</i> -C ₆ H ₄ Cl ₂	525	568	0.76	1440
	CH ₂ Cl ₂	522	566	0.58	1490
	MeCN	520	569	0.075	1660
39	<i>o</i> -C ₆ H ₄ Cl ₂	535	586	0.63	1630
	CH ₂ Cl ₂	531	582	0.59	1650
	MeCN	528	590	0.20	1990
40	<i>o</i> -C ₆ H ₄ Cl ₂	547	593	0.69	1420
	CH ₂ Cl ₂	541	593	0.46	1620
	MeCN	537	592	0.17	1730
41	<i>o</i> -C ₆ H ₄ Cl ₂	553	604	0.64	1530
	CH ₂ Cl ₂	546	604	0.43	1760
	MeCN	543	609	0.18	2000
42	<i>o</i> -C ₆ H ₄ Cl ₂	575	669	0.12	2440
	CH ₂ Cl ₂	565	670	0.02	2770
	MeCN	557	688	0.04	3420
43	<i>o</i> -C ₆ H ₄ Cl ₂	555	598	598	980
	CH ₂ Cl ₂	548	592	592	1160
	MeCN	544	592	592	1490
43 ^{mono}	<i>o</i> -C ₆ H ₄ Cl ₂	532	575	—	1420
	CH ₂ Cl ₂	527	552	—	1020

Table 10 (Contd.)

Dye	Solvent	λ_{abs} [nm]	λ_{em} [nm]	Φ_{fl}	$\Delta\nu$ [cm ⁻¹]
44	MeCN	522	561	—	1360
	<i>o</i> -C ₆ H ₄ Cl ₂	551	595	0.06	1360
	CH ₂ Cl ₂	545	594	—	1500
44 ^{mono}	MeCN	542	589	—	1480
	<i>o</i> -C ₆ H ₄ Cl ₂	527	569	0.02	1400
	CH ₂ Cl ₂	524	551	—	940
45 ^{mono}	MeCN	521	565	—	1500
	<i>o</i> -C ₆ H ₄ Cl ₂	527	569	—	1400
	CH ₂ Cl ₂	524	562	—	1290
	MeCN	522	559	—	1270

significantly to fluorescence modulation. As an example, placing either Me or OMe group at the *ortho* position relative to the DPND core increases emission intensity (*i.e.* 35 *vs.* 36) by hindering rotation around C_{aryl}–C_{DPND} bond. Those groups may also affect electronic distribution *via* both inductive and mesomeric effects. As a matter of fact, careful structure optimization by taking into account all of these factors allowed us to describe nitroaromatics featuring enormous value of Φ_{fl} (up to 0.96), even in relatively polar dichloromethane (28 or 36).

The origin of the specific dependence of emission intensity on solvent polarity was investigated^{30b} by means of theoretical calculations which revealed surprising, aborted photochemical reactivity after photoexcitation (Fig. 19 and 20). The fluorescence in the series of DPND-based nitroaromatics clearly comes from deexcitation of the lowest in energy S₁ (1 π –1 π^*) state. However, the S₁ state may also adiabatically relaxed *via* a transition to ¹CT (*ortho*- or *peri*-NO₂ isomers) or ¹np* (*para*- or *meta*-NO₂ isomers) states. Then, these states efficiently undergo non-radiative depopulation *via* a conical intersection (CI) with the S₀ state.

Theoretical results also suggest that the nitro group twists upon photoexcitation around the C_{DPND}–N_{nitro} bond with subsequent formation of a new, covalent C_{DPND}–O_{nitro} bond in ¹CT and ¹np* states. The formation of a new bond with more polar character tends to occur much easier in polar environment. Then, this bond breaks when transitioning from the CI to the more favourable ground-state configuration during relaxation. This phenomenon is called the aborted photochemistry (Fig. 19 and 20).⁴⁹

Two-photon absorption (TPA) in DPNDs

Two-photon absorption (TPA) phenomenon⁵⁰ have found multiple, real-life applications such as 3D imaging of materials,⁵¹ microfabrication and photopolymerization,⁵² photopharmacology⁵³ or imaging of biological tissues.⁵⁴ An efficient TPA absorber should feature a long system of conjugated multiple bonds and contain donor and acceptor groups that potentially would participate in the formation of strongly polarized charge-transfer states.⁵⁵ As a completely new chromophore, the DPND core was investigated as a TPA absorber for



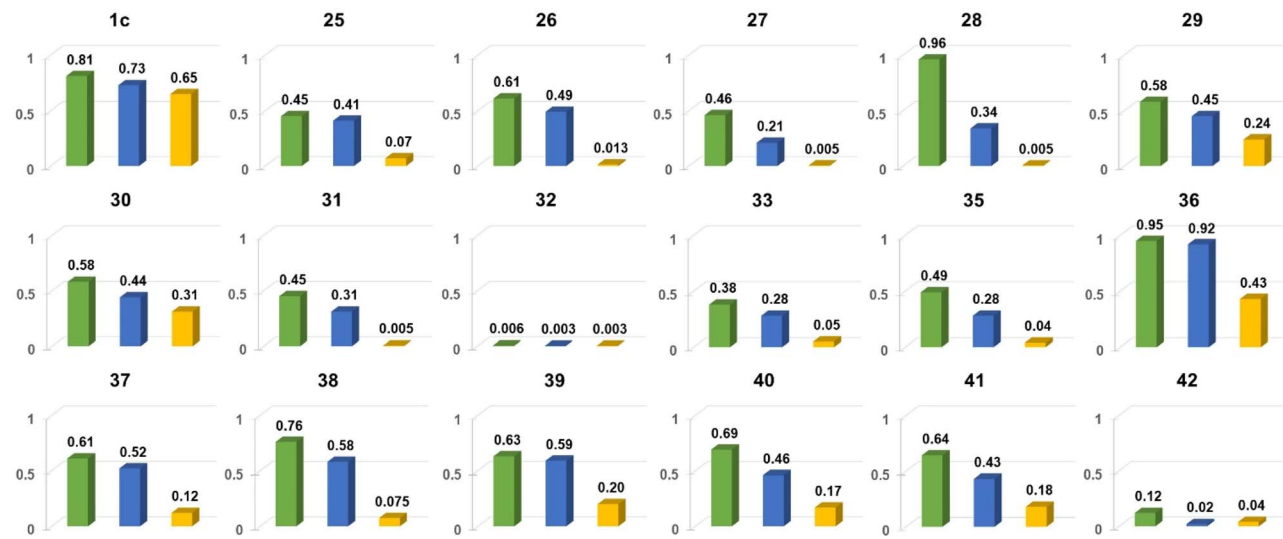


Fig. 18 Comparison of Φ_{fl} for chosen nitroaromatics bearing the DPND core in three different solvents: 1,2-dichlorobenzene (green), CH_2Cl_2 (blue) and MeCN (orange). Adapted with permission from ref. 48. Copyright 2023 Royal Society of Chemistry.

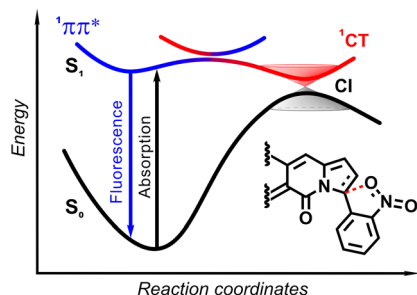


Fig. 19 Schematic diagram showing the scenario of temporal evolution of the photoexcited *ortho*-nitrophenyl substituted DPND. The electrons are initially photoexcited to locally excited (LE) state (${}^1\pi-\pi^*$) and is non-adiabatically transferred to the CT state along the reaction coordinate. The photoexcited system recombines radiatively from S_1 to S_0 or nonradiatively through ${}^1\pi-\pi^* \rightarrow {}^1\text{CT} \rightarrow S_0$ transitions. Cl – conical intersection. Adapted with permission from ref. 30b. Copyright 2021 Royal Society of Chemistry.

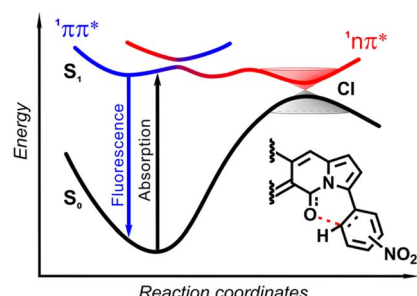


Fig. 20 Schematic diagram showing the general scenario of temporal evolution of the photoexcited *meta*- and *para*-nitrophenyl substituted DPNDs. The system is initially photoexcited to the ${}^1\pi-\pi^*$ state and is non-adiabatically transferred to the ${}^1n-\pi^*$ state along the reaction coordinate. The photoexcited system recombines radiatively from S_1 to S_0 or nonradiatively through ${}^1\pi-\pi^* \rightarrow {}^1n-\pi^* \rightarrow S_0$ transitions. Cl – conical intersection. Adapted with permission from ref. 30b. Copyright 2021 Royal Society of Chemistry.

the first time already in 2018.²⁷ We have found out that dyes bearing double- or triple-bond linkages between the DPND core and flanking aryl rings exhibit superior values of two-photon absorption cross-sections (σ_2^{max}) (Table 11), where the highest value of σ_2^{max} was noted for compound **11a** bearing a double-bond linkage between the DPND core and nitroaryl flanking

Table 11 Two-photon absorption data for chosen, nitro-decorated DPNDs in CH_2Cl_2

Dye	$\lambda_{2\text{PA}}^{\text{max}}/\text{nm}$	$\sigma_2^{\text{max}}/\text{GM}$	$\sigma_2^{\text{max}} \varphi_{\text{fl}}/\text{GM}$	$\sigma_2^{\text{max}}/\text{MW}^c$
1c^a	750	44	32	<1
11a^b	820	5180	83	9.3
11b^b	740	5100	112	9.8
11c^b	740	1710	70	3.2
12a^b	720	2840	1450	5.1
12b^b	720	850	500	1.6
12c^b	860	1990	340	3.6
25^a	<690	>3718	>1524	7.3
26^a	<680	312	153	<1
27^a	<690	>835	>175	1.5
28^a	<680	>197	>67	<1
29^a	<690	>1177	>530	2.2
30^a	<690	>1326	>583	2.3
31^a	<690	>1134	>352	1.8
32^a	<690	>9	0	0
33^a	720	1384	388	2.1
35^a	<680	>233	>65	<1
36^a	<685	>175	>161	<1
37^a	<685	>167	>87	<1
38^a	<685	>96	>56	<1
39^a	<685	≥ 161	≥ 95	<1
40^a	<680	>340	>156	<1
41^a	<700	≥ 513	≥ 221	<1
42^a	755	104	2	<1

^a Determined using the two-photon excited fluorescence (TPEF) technique.⁵⁶ ^b Determined using Z-scan setup.⁵⁷ ^c The molecular weights were calculated by replacing alkyl groups at positions 6 and 12 by a methyl group (CH_3).



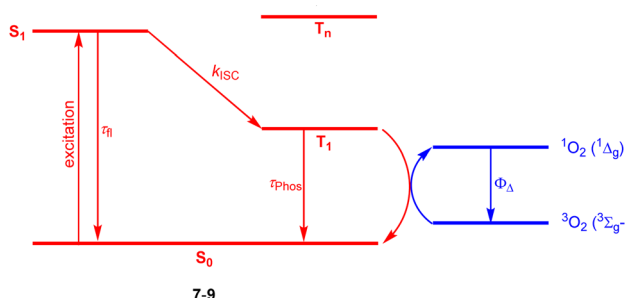


Fig. 21 Schematic illustration of energy levels and triplet sensitization in 7–9.^{21,60}

Table 12 Summary of the lifetimes, rate constants of these processes extracted from the ns-TA and fs-TA experiments

Dye	τ_{fl}/ns	k_{ISC}/s^{-1}	$\tau_T/\mu\text{s}$	τ_{Phos}/ms	$\Phi_\Delta/\%$
7a	5.1	—	5.1	8.2	31
8	5.7	1.6×10^8	16	7.9	28
9	0.34	2.9×10^9	0.31	9.0	52

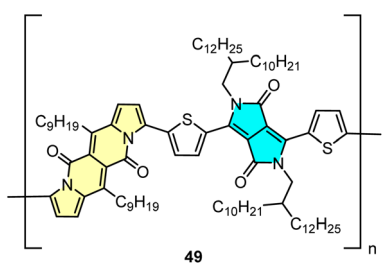


Fig. 22 The structure of polymer 49.

moieties ($\sigma_2^{\text{max}} = 5180 \text{ GM}$). Notably, while compounds from both series (**11** and **12**) possessed a beneficial ratio of $\sigma_2^{\text{max}}/\text{MW}$ (1.6–9.8 GM g⁻¹), dyes of type **12** show high values of two-photon brightness $\sigma_2^{\text{max}} \cdot \Phi_b$, which is an important feature from the viewpoint of bioimaging applications.^{55b}

Later on, we carefully evaluated weakly-coupled bis-arylated DPNs derivatives containing nitroaryl moieties as potential TPA absorbers (Scheme 4 and Table 11).⁴⁸ Weak electronic communication between the nitro group auxochrome and the DPNs core resulted in weaker non-linear response compared with **11a** or **12a**. Among compounds tested, **25** showed a reasonable TPA response ($\sigma_2^{\text{max}} > 1524 \text{ GM}$) whereas other derivatives performed weaker ($\sigma_2^{\text{max}} < 600 \text{ GM}$) in the accessible spectral window size.⁴⁸

DPNDs as triplet sensitizers

Halogenation is the most established strategy to intensify population of a triplet excited state⁵⁸ due to enhanced spin-orbit coupling (SOC).⁵⁹ Such halogenated derivatives have been widely studied and as emerging agents for photodynamic therapy (PDT). Along this strategy, Ayitou and others tested halogenated DPNs (**7–9**) as potential (PDT) agents (Fig. 21 and Table 12).^{21,60} The presence of heavy halogen atoms within the DPNs core was believed to enhance spin-orbit coupling (SOC) dynamics, thus leading to efficient singlet oxygen ($^1\text{O}_2$) production. They found that all halogen-substituted dyes do produce $^1\text{O}_2$ with admirable efficiencies and the highest value of Φ_Δ was determined for **9**. Surprisingly, values of fluorescence quantum yields measured for **7c** and **8** (75 and 76%, respectively) are comparable to the value measured for **1c**, although they bear chlorine and bromine atoms within the core.

DPND-based polymer as a potential material for OFETs

Direct arylation methodology appeared to be useful in the preparation of polymer **49** in one step from the DPNs core and dibrominated derivative bearing the diketopyrrolopyrrole (DPP) unit (Fig. 22).³² The weight-average molecular weight (M_w) and polydispersity index (PD) determined by HT-GPC were 77.7 kDa and 2.64, respectively, while the UV-VIS spectrum recorded in toluene showed a strong absorption band in the NIR region with $\lambda_{\text{max}} = 866 \text{ nm}$. Polymer **49** was examined by BASF as a potential electron transport material in OFETs, nevertheless a particularly low value of electron mobility ($\mu = 8.85 \times 10^{-12} \text{ cm}^2 \text{ V}^{-1} \text{ m}^{-1}$) was measured.

5. Summary and outlook

Although the history of cross-conjugated dyes dates back to the ancient times, still there are numerous possible structures that have never been either assembled or investigated. In seven years which elapsed since their discovery, dipyrrrolonaphthalimidinediones made a notable impact on chemistry. Their straightforward synthesis combined with functionalization possibilities are responsible for the quick initial progress in terms of structural exploitation. In the second phase the deciding factor turned out to be their intriguing photophysical characteristics and in particular: (1) strong and easily tunable emission; (2) low energy of T_1 excited state which enables singlet fission in the crystalline state; (3) large two-photon absorption cross-sections after derivatization. Studies on dipyrrrolonaphthalimidinediones: (1) were the deciding factor enabling formulation of strategies towards strongly fluorescent nitroaromatics; (2) provided the shortest pathway to twist-acenes; (3) delivered dyes with large optical brightness and exceptionally high values of two-photon absorption cross-section divided by molecular mass. Notwithstanding their success, there are still numerous synthetic limitations which have to be overcome in the nearest future to ensure continuous progress. The main envisioned areas for synthetic explorations are as follows: (1) preparation of DPNs directly from aromatic acids; (2) extension of the DPNs' synthesis to embrace such



substrates as indole, isoindole *etc.*; (3) transformation of DPNDs into polar, water-soluble probes. In 2016 it would be impossible to imagine that only seven years later the chemistry of DPNDs would expand to create independent field of study within the chemistry of functional dyes. One can venture hypothesis that once these synthetic limitations are overcome these new π -expanded DPNDs could witness rapid development. The analysis of research performed within the last few years suggest that the number of known as well as possible structures of cross-conjugated nature is limited only by our imagination.

Author contributions

All authors contributed to the conceptualization. B. S. performed literature search, wrote the first draft and made all schemes/figures. All authors were involved in revising, editing, and proofreading.

Conflicts of interest

There are no conflicts to declare.

Acknowledgements

The work was financially supported by the Polish National Science Centre (Sonata 2021/43/D/ST4/02267 and OPUS 2020/37/B/ST4/00017). This project has received funding from EU's Horizon 2020 research and innovation programme under Grant Agreement No. 860762. Authors thank Dr Marek Grzybowski for discovering DPNDs.

References

- (a) N. Singh, S. Singh, S. Kohli, A. Singh, H. Asiki, G. Rathee, R. Chandra and E. A. Anderson, *Org. Chem. Front.*, 2021, **8**, 5550–5573; (b) J. T. Gupton, in *Heterocyclic Antitumor Antibiotics*, ed. M. Lee, Springer Berlin Heidelberg, Berlin, Heidelberg, 2006, pp. 53–92.
- (a) V. Bhardwaj, D. Gumber, V. Abbot, S. Dhiman and P. Sharma, *RSC Adv.*, 2015, **5**, 15233–15266; (b) G. Li Petri, V. Spanò, R. Spatola, R. Holl, M. V. Raimondi, P. Barraja and A. Montalbano, *Eur. J. Med. Chem.*, 2020, **208**, 112783.
- (a) J. Kim, J. Oh, A. Osuka and D. Kim, *Chem. Soc. Rev.*, 2022, **51**, 268–292; (b) B. Szyszko, M. J. Bialek, E. Pacholska-Dudziak and L. Latos-Grajynski, *Chem. Rev.*, 2017, **117**, 2839–2909.
- R. Orłowski, D. Gryko and D. T. Gryko, *Chem. Rev.*, 2017, **117**, 3102–3137.
- B. Sadowski, J. Klajn and D. T. Gryko, *Org. Biomol. Chem.*, 2016, **14**, 7804–7828.
- (a) C. Bellomo, M. Chaari, J. Cabrera-González, M. Blangetti, C. Lombardi, A. Deagostino, C. Viñas, N. Gaztelumendi, C. Nogués, R. Nufiez and C. Prandi, *Chem.-Eur. J.*, 2018, **24**, 15622–15630; (b) A. Loudet and K. Burgess, *Chem. Rev.*, 2007, **107**, 4891–4932.
- (a) A. N. Bismillah and I. Aprahamian, *Chem. Soc. Rev.*, 2021, **50**, 5631–5649; (b) S. Boodts, E. Fron, J. Hofkens and W. Dehaen, *Coord. Chem. Rev.*, 2018, **371**, 1–10; (c) I.-S. Tamgho, A. Hasheminasab, J. T. Engle, V. N. Nemykin and C. J. Ziegler, *J. Am. Chem. Soc.*, 2014, **136**, 5623–5626.
- (a) W. Zeng, O. El Bakouri, D. W. Szczepanik, H. Bronstein and H. Ottosson, *Chem. Sci.*, 2021, **12**, 6159–6171; (b) W. Zeng, D. W. Szczepanik and H. Bronstein, *J. Phys. Org. Chem.*, 2023, **36**, e4441; (c) M. Swart, *Theor. Chem. Acc.*, 2020, **139**; (d) L. Wang, L. Lin, J. Yang, Y. Wu, H. Wang, J. Zhu, J. Yao and H. Fu, *J. Am. Chem. Soc.*, 2020, **142**, 10235–10239.
- (a) A. Borissov, Y. K. Maurya, L. Moshniah, W.-S. Wong, M. Żyła-Karwowska and M. Stępień, *Chem. Rev.*, 2022, **122**, 565–788; (b) M. Stępień, E. Gońska, M. Żyła and N. Sprutta, *Chem. Rev.*, 2017, **117**, 3479–3716.
- M. Grzybowski and D. T. Gryko, *Adv. Opt. Mater.*, 2015, **3**, 280–320.
- R. Stalder, J. Mei, K. R. Graham, L. A. Estrada and J. R. Reynolds, *Chem. Mater.*, 2014, **26**, 664–678.
- J. Kaleta, M. Dudić, L. Ludvíková, A. Liška, A. Zaykov, I. Rončević, M. Mašát, L. Bednárová, P. I. Dron, S. J. Teat and J. Michl, *J. Org. Chem.*, 2023, **88**, 6573–6587.
- (a) A. D. Hendsbee, J.-P. Sun, L. R. Rutledge, I. G. Hill and G. C. Welch, *J. Mater. Chem. A*, 2014, **2**, 4198–4207; (b) M. Vatanparast and Z. Shariatinia, *Sol. Energy*, 2021, **230**, 260–268; (c) B. He, A. B. Pun, D. Zhrebetsky, Y. Liu, F. Liu, L. M. Klivansky, A. M. McGough, B. A. Zhang, K. Lo, T. P. Russell, L. Wang and Y. Liu, *J. Am. Chem. Soc.*, 2014, **136**, 15093–15101.
- C. Du, S. Fu, X. Ren, X. Wang, Z. Wang, J. Zhou and H. Wang, *New J. Chem.*, 2018, **42**, 3493–3502.
- (a) E. D. Głowacki, G. Voss, L. Leonat, M. Irimia-Vladu, S. Bauer and N. S. Sariciftci, *Isr. J. Chem.*, 2012, **52**, 540–551; (b) R. J. H. Clark, C. J. Cooksey, M. A. M. Daniels and R. Withnall, *Endeavour*, 1993, **17**, 191–199.
- D. G. Farnum, G. Mehta, G. G. I. Moore and F. P. Siegal, *Tetrahedron Lett.*, 1974, **15**, 2549–2552.
- (a) J. Pfenninger, A. Iqbal, A. C. Rochat, O. Wallquist and A. G. Ciba-Geigy, *Eur. Pat. Appl.* 184982, 1986; (b) A. Iqbal and L. Cassar, Ciba-Geigy Corporation, *US Pat.* 4415685, 1983; (c) L. Cassar, A. Iqbal, A. C. Rochat and A. G. Ciba-Geigy, *Eur. Pat. Appl.* 98808, 1983.
- M. Grzybowski, I. Deperasińska, M. Chotkowski, M. Banasiewicz, A. Makarewicz, B. Kozankiewicz and D. T. Gryko, *Chem. Commun.*, 2016, **52**, 5108–5111.
- L. Wang, W. Cai, J. Sun, Y. Wu, B. Zhang, X. Tian, S. Guo, W. Liang, H. Fu and J. Yao, *J. Phys. Chem. Lett.*, 2021, **12**, 12276–12282.
- B. Sadowski, D. Mierzwa, S. Kang, M. Grzybowski, Y. M. Poronik, A. L. Sobolewski, D. Kim and D. T. Gryko, *Chem. Commun.*, 2022, **58**, 3697–3700.
- J. Morgan, Y. J. Yun, A. M. Jamhawi, S. M. Islam and A. J.-L. Ayitou, *Photochem. Photobiol.*, 2023, **99**, 761–768.
- C. Song, D. W. Knight and M. A. Whatton, *Tetrahedron Lett.*, 2004, **45**, 9573–9576.
- (a) J. I. Ayogu and E. A. Onoabedje, *Catal. Sci. Tech.*, 2019, **9**, 5233–5255; (b) K. H. Shaughnessy, in *Metal-Catalyzed Reactions in Water*, Wiley, 2013, pp. 1–46; (c) R. Chinchilla



and C. Nájera, *Chem. Rev.*, 2007, **107**, 874–922; (d) S. E. Hooshmand, B. Heidari, R. Sedghi and R. S. Varma, *Green Chem.*, 2019, **21**, 381–405.

24 (a) L. I. Belen'kii, T. G. Kim, I. A. Suslov and N. D. Chuvylkin, *Arkivoc*, 2003, 59–67; (b) S. Nomiyama, T. Ogura, H. Ishida, K. Aoki and T. Tsuchimoto, *J. Org. Chem.*, 2017, **82**, 5178–5197; (c) D. Ghorai and G. Mani, *Inorg. Chem.*, 2014, **53**, 4117–4129; (d) T. Buchała, A. Chudoba and S. Roszak, *Struct. Chem.*, 2016, **27**, 185–189.

25 (a) Y. Gao, C. Feng, T. Seo, K. Kubota and H. Ito, *Chem. Sci.*, 2022, **13**, 430–438; (b) B. Godlewski, D. Baran, M. De Robichon, A. Ferry, S. Ostrowski and M. Malinowski, *Org. Chem. Front.*, 2022, **9**, 2396–2404.

26 T. Rohand, W. Qin, N. Boens and W. Dehaen, *Eur. J. Org. Chem.*, 2006, 4658–4663.

27 B. Sadowski, H. Kita, M. Grzybowski, K. Kamada and D. T. Gryko, *J. Org. Chem.*, 2017, **82**, 7254–7264.

28 B. Sadowski, M. Loebnitz, D. R. Dombrowski, D. H. Friese and D. T. Gryko, *J. Org. Chem.*, 2018, **83**, 11645–11653.

29 P. G. Chirila and C. J. Whiteoak, *Dalton Trans.*, 2017, **46**, 9721–9739.

30 (a) B. Sadowski, M. F. Rode and D. T. Gryko, *Chem.-Eur. J.*, 2018, **24**, 855–864; (b) B. Sadowski, M. Kaliszewska, Y. M. Poronik, M. Czichy, P. Janasik, M. Banasiewicz, D. Mierzwa, W. Gadomski, T. D. Lohrey, J. A. Clark, M. Lapkowski, B. Kozankiewicz, V. I. Vullev, A. L. Sobolewski, P. Piatkowski and D. T. Gryko, *Chem. Sci.*, 2021, **12**, 14039–14049; (c) B. Sadowski, S.-H. Su, T.-C. Lin, T. D. Lohrey, I. Deperasińska, P.-T. Chou and D. T. Gryko, *J. Mater. Chem. C*, 2018, **6**, 12306–12313.

31 (a) H. Bohra and M. Wang, *J. Mater. Chem. A*, 2017, **5**, 11550–11571; (b) X. Wang, Y. Li, J. Li, Y. Zhang, J. Shao and Y. Li, *Molecules*, 2023, **28**, 3515; (c) I. A. Stepek and K. Itami, *ACS Mater. Lett.*, 2020, **2**, 951–974.

32 M. Grzybowski, D. T. Gryko, B. Sadowski, K. Strassel, D. Kaelblein and P. Hayoz, Polymers and compounds based on dipyrrolo[1,2-b:1',2'-g][2,6]naphthyridine-5,11-dione, International Pat no. WO2017068009, 2018.

33 B. Sadowski, D. J. Stewart, A. T. Phillips, T. A. Grusenmeyer, J. E. Haley, T. M. Cooper and D. T. Gryko, *J. Org. Chem.*, 2020, **85**, 284–290.

34 S. Ito, S. Hiroto and H. Shinokubo, *Org. Lett.*, 2013, **15**, 3110–3113.

35 J. O. Morley, *Int. J. Quantum Chem.*, 1993, **46**, 19–26.

36 P. J. McCartin, *J. Chem. Phys.*, 2004, **42**, 2980–2981.

37 (a) Y. Hong, J. W. Y. Lam and B. Z. Tang, *Chem. Commun.*, 2009, 4332–4353; (b) Y. Hong, J. W. Y. Lam and B. Z. Tang, *Chem. Soc. Rev.*, 2011, **40**, 5361.

38 L. A. Estrada, R. Stalder, K. A. Abboud, C. Risko, J.-L. Brédas and J. R. Reynolds, *Macromolecules*, 2013, **46**, 8832–8844.

39 J. Dhar, N. Venkatramiah and S. Patil, *J. Mater. Chem. C*, 2014, **2**, 3457–3466.

40 (a) D. Bialas, S.-L. Suraru, R. Schmidt and F. Würthner, *Org. Biomol. Chem.*, 2011, **9**, 6127–6132; (b) S. Luňák, P. Horáková and A. Lyčka, *Dyes Pigm.*, 2010, **85**, 171–176.

41 (a) M. B. Smith and J. Michl, *Chem. Rev.*, 2010, **110**, 6891–6936; (b) M. B. Smith and J. Michl, *Annu. Rev. Physiol.*, 2013, **64**, 361–386.

42 J. Xia, S. N. Sanders, W. Cheng, J. Z. Low, J. Liu, L. M. Campos and T. Sun, *Adv. Mater.*, 2017, **29**, 1601652.

43 A. Rao and R. H. Friend, *Nat. Rev. Mater.*, 2017, **2**, 17063.

44 L. Wang, Y. Wu, Y. Liu, L. Wang, J. Yao and H. Fu, *J. Chem. Phys.*, 2019, 151.

45 K. J. Fallon, P. Budden, E. Salvadori, A. M. Ganose, C. N. Savory, L. Eyre, S. Dowland, Q. Ai, S. Goodlett, C. Risko, D. O. Scanlon, C. W. M. Kay, A. Rao, R. H. Friend, A. J. Musser and H. Bronstein, *J. Am. Chem. Soc.*, 2019, **141**, 13867–13876.

46 Y. Wu, L. Lu, B. Yu, S. Zhang, P. Luo, M. Chen, J. He, Y. Li, C. Zhang, J. Zhu, J. Yao and H. Fu, *J. Phys. Chem. Lett.*, 2023, **14**, 4233–4240.

47 (a) Y. M. Poronik, B. Sadowski, K. Szycita, F. H. Quina, V. I. Vullev and D. T. Gryko, *J. Mater. Chem. C*, 2022, **10**, 2870–2904; (b) M.-C. Chen, D.-G. Chen and P.-T. Chou, *ChemPlusChem*, 2021, **86**, 11–27; (c) W. Rodriguez-Cordoba, L. Gutierrez-Arzaluz, F. Cortes-Guzman and J. Peon, *Chem. Commun.*, 2021, **57**, 12218–12235.

48 B. Sadowski, M. Kaliszewska, G. Clermont, Y. M. Poronik, M. Blanchard-Desce, P. Piatkowski and D. T. Gryko, *Chem. Commun.*, 2023, **59**, 11708–11711.

49 (a) A. Sinicropi, W. M. Nau and M. Olivucci, *Photochem. Photobiol.*, 2002, **1**, 537–546; (b) D. Shemesh, A. L. Sobolewski and W. Domcke, *J. Am. Chem. Soc.*, 2009, **131**, 1374–1375; (c) D. Tuna, A. L. Sobolewski and W. Domcke, *Phys. Chem. Chem. Phys.*, 2014, **16**, 38–47.

50 M. Göppert-Mayer, *Ann. Phys.*, 1931, **401**, 273–294.

51 C. Dorfer, D. Hits, L. Kasmi, G. Kramberger, M. Lucchini, M. Mikuž and R. Wallny, *Appl. Phys. Lett.*, 2019, 114.

52 (a) S. Maruo, O. Nakamura and S. Kawata, *Opt. Lett.*, 1997, **22**, 132–134; (b) Z. Faraji Rad, P. D. Prewett and G. J. Davies, *Microsyst. Nanoeng.*, 2021, **7**, 71; (c) S. O'Halloran, A. Pandit, A. Heise and A. Kellett, *Adv. Sci.*, 2023, **10**, 2204072.

53 M. Izquierdo-Serra, M. Gascón-Moya, J. J. Hirtz, S. Pittolo, K. E. Poskanzer, È. Ferrer, R. Alibés, F. Busqué, R. Yuste, J. Hernando and P. Gorostiza, *J. Am. Chem. Soc.*, 2014, **136**, 8693–8701.

54 (a) F. Helmchen and W. Denk, *Nat. Methods*, 2005, **2**, 932–940; (b) G. Sancataldo, O. Barrera and V. Vetrí, in *Principles of Light Microscopy: From Basic to Advanced*, ed. V. Nechyporuk-Zloy, Springer International Publishing, Cham, 2022, pp. 215–241.

55 (a) M. Pawlicki, H. A. Collins, R. G. Denning and H. L. Anderson, *Angew. Chem., Int. Ed.*, 2009, **48**, 3244–3266; (b) H. Myung Kim and B. R. Cho, *Chem. Commun.*, 2009, 153–164.

56 (a) M. A. Albota, C. Xu and W. W. Webb, *Appl. Opt.*, 1998, **37**, 7352–7356; (b) C. Xu and W. W. Webb, *J. Opt. Soc. Am. B*, 1996, **13**, 481–491.

57 K. Kamada, K. Matsunaga, A. Yoshino and K. Ohta, *J. Opt. Soc. Am. B*, 2003, **20**, 529–537.



58 (a) J. Grüne, G. Londi, A. J. Gillett, B. Stähly, S. Lulei, M. Kotova, Y. Olivier, V. Dyakonov and A. Sperlich, *Adv. Funct. Mater.*, 2023, **33**, 2212640; (b) W. Hu, R. Zhang, X.-F. Zhang, J. Liu and L. Luo, *Part*, 2022, **272**, 120965.

59 (a) M. Fagnoni, *Angew. Chem., Int. Ed.*, 2010, **49**, 6709–6710; (b) C. M. Marian, *Wiley Interdiscip. Rev. Comput. Mol. Sci.*, 2012, **2**, 187–203.

60 J. Morgan, Y. J. Yun and A. J.-L. Ayitou, *Photochem. Photobiol.*, 2022, **98**, 57–61.

